Inorganic Chemistry
Article

*Inorg. Chem.* **2009**, *48*, 8897–8910 **8897**
DOI: 10.1021/ic901133k

# Construction of Metal−Organic Oxides from Molybdophosphonate Clusters and Copper-Bipyrimidine Building Blocks

**N. Gabriel Armatas,[†] Wayne Ouellette,[†] Kelly Whitenack,[†] Joshua Pelcher,[†] Hongxue Liu,[‡] Erin Romaine,[‡] Charles J. O'Connor,[‡] and Jon Zubieta*[,†]**

[†]*Department of Chemistry, Syracuse University, Syracuse, New York 13244, and* [‡]*Department of Chemistry, University of New Orleans, New Orleans, Louisiana 70148*

Received June 11, 2009

A series of organic−inorganic hybrid materials of the copper(II)-molybdophosphonate family have been prepared using conventional hydrothermal conditions. The reactions of $MoO_3$, copper(II) acetate, bipyrimidine (bpyr), a phosphonic acid, and water at temperatures below 160 °C and in the presence of a mineralizer such as acetic acid or HF provided crystalline samples of materials of the general class $\{Cu_2(bpyr)\}^{4+}/Mo_xO_y$-phosphonate. The recurrent themes of the structures are the presence of the binuclear $\{Cu_2(bpyr)\}^{4+}$ and pentanuclear $\{Mo_5O_{15}(O_3PR)_2\}^{4-}$ building blocks. For the alkylphosphonate-containing materials, $[\{Cu_2(bpyr)_2\}Mo_5O_{15}(O_3PCH_3)_2]\cdot 2.5H_2O$ (**1**·2.5$H_2O$) is two-dimensional and exhibits $\{Cu(bpyr)\}_n^{2n+}$ chains, while $[\{Cu_2(bpyr)(H_2O)\}Mo_5O_{15}(O_3PCH_2CH_3)_2]$ (**2**) is three-dimensional. The diphosphonate series of materials $\{\{Cu_2(bpyr)\}^{4+}[Mo_5O_{15}\{O_3P(CH_2)_nPO_3\}]^{4-}$ with $n = 2-6$ (**4**, **5**, **7**−**9**) in all cases contain the characteristic $[Mo_5O_{15}\{O_3P(CH_2)_nPO_3\}]_n^{2n+}$ chains, linked through $\{Cu_2(bpyr)\}^{4+}$ rods into three-dimensional frameworks. When $n = 1$, the three-dimensional phase $[\{Cu_2(bpyr)\}MoO_2(HO_3PCH_2PO_3)_2]\cdot 2H_2O$ (**3**·2$H_2O$) is obtained, the exclusive example of a structure constructed from isolated $\{MoO_6\}$ polyhedra rather than pentamolybdate clusters. The Ni(II)-containing phase $[\{Ni_2(bpyr)(H_2O)_4\}Mo_5O_{15}\{O_3P(CH_2)_3PO_3\}]\cdot 9H_2O$ (**6**·9$H_2O$) was also prepared and compared to the structure of the Cu(II) analogue, $[\{Cu_2(bpyr)(H_2O)_4\}Mo_5O_{15}\{O_3P(CH_2)_3PO_3\}]\cdot 3H_2O$ (**5**·3$H_2O$). Magnetic susceptibility studies of the compounds revealed that the magnetic behavior was consistent in all cases with antiferromagnetically coupled dimers. However, the magnitude of the exchange coupling was clearly dependent on the orientation of the M(II) mean equatorial or basal planes relative to the bipyrimidine plane. Thus, when the metal and bipyrimidine planes are nearly coplanar, the *J* values are in the −77 to −87 $cm^{-1}$ range, while *J* values of −2 to −5 $cm^{-1}$ are observed for the compounds with out-of-plane orientations.

The significant contemporary interest in inorganic oxides reflects their structural and compositional diversity, as well as their applications to sorption, separations, catalysis, and solar energy conversion.[1−11] The fundamental and practical importance of these materials drives efforts to develop methods for the rational design of inorganic oxide structures.[12−15]

The building block approach adopts the strategy of linking molecular oxide clusters through organic tethers or secondary metal−ligand subunits.[12−20] Our strategies exploit the use of chemically robust and structurally diverse

*To whom correspondence should be addressed. E-mail: jazubiet@syr.edu.

(1) Greenwood, N. N.; Earnshaw, A. *Chemistry of the Elements*; Pergamon Press: New York, 1984.
(2) Wells, A. F. *Structural Inorganic Chemistry*, 4th ed.; Oxford University Press: Oxford, U. K., 1978.
(3) McCarroll, W. H. *Encyclopedia of Inorganic Chemistry*; King, R. B., Ed.; John Wiley & Sons: New York, 1994; Vol. *6*, pp 2903−2946.
(4) Bruce, D. W.; O'Hare, D. *Inorganic Materials*; Wiley: Chichester, U. K., 1992.
(5) Cheetham, A. K. *Science* **1964**, *264*, 794.
(6) Cockayne, B.; James, D. W. *Modern Oxide Materials*; Academic Press; New York, 1972.
(7) Büchner, W.; Schliebs, R.; Winter, G.; Büchel, K. H. *Industrial Inorganic Chemistry*; VCH: New York, 1989.
(8) Okuhara, T.; Misono, M. *Encyclopedia of Inorganic Chemistry*; John Wiley and Sons: New York, 1994; Vol. *6*, p 2889.
(9) Clearfield, A. *Chem. Rev.* **1988**, *88*, 125.
(10) Newsam, J. M. *Solid State Compounds*; Clarendon Press: Oxford, 1992; p 234.
(11) Landau, M. V. Transition Metal Oxides. In *Handbook of Porous Solids*; Wiley-VCH: Weinheim, Germany, 2002; vol. *3*, pp 1677−1765.
(12) Hagrman, P. J.; Hagrman, D.; Zubieta, J. *Angew. Chem., Int. Ed. Engl.* **1999**, *38*, 2638.
(13) DeBord, J. R. D.; Haushalter, R. C.; Meyer, C. M.; Rose, D. J.; Zapf, P. J.; Zubieta, J. *Inorg. Chim. Acta* **1997**, *256*, 165.
(14) Khan, M. I.; Yohannes, E.; Doedens, R. J. *Angew. Chem., Int. Ed. Engl.* **1999**, *38*, 1292.
(15) Khan, M. I.; Yohannes, E.; Doedens, R. J. *Inorg. Chem.* **2003**, *42*, 3125 and references therein.
(16) Chen, J.; Lu, S.; Yu, R.; Chen, Z.; Huang, Z.; Lu, C. *Chem. Commun.* **2002**, 2640.
(17) Linnard, L.; Dolbecq, A.; Mialene, P.; Marrot, J.; Secheresse, F. *Inorg. Chem. Acta.* **2004**, *357*, 845.
(18) Farrette, S.; Hasenknopf, B.; Vaissermann, J.; Gouzerh, P.; Roux, C. *Chem. Commun.* **2003**, 2664.
(19) Lin, B. Z.; Chen, Y.-M.; Liu, P.-D. *Dalton Trans.* **2003**, 2474.
(20) Finn, R. C.; Sims, J.; O'Connor, C. J.; Zubieta, J. *J. Chem. Soc., Dalton Trans.* **2002**, *159* and references therein.

© 2009 American Chemical Society
Published on Web 08/17/2009

polyoxometalate clusters[21−26] as nodes from which organic or metal−organic tethers radiate in more or less predictable fashion to provide spatial expansion. Complex structures have been derived from Keggin-,[27−31] Anderson-,[32,33] Silverton-,[34] and Wells-Dawson-type[35−37] polyoxoanions.

We have adopted an approach that uses oxomolybdenum organophosphonate clusters as nodes with organic tethers and secondary metal coordination complex cations as spokes to link the nodes into one-, two-, or three-dimensional materials.[38−46] The pentamolybdate $[Mo_5O_{15}(O_3PR)_2]^{4-}$ or hexamolybdate $[Mo_6O_{18}(O_3AsR)_2]^{4-}$ clusters[47−49] can be tethered through the organic chains of diphosphonate $\{O_3P\text{-tether-}PO_3\}^{4-}$ or diarsonate $\{O_3As\text{-tether-}AsO_3\}^{4-}$ groups. Metal−diphosphonate materials are prototypical organic−inorganic hybrid composites that have been extensively investigated.[50−56] The tether length and tether type are readily modified, and additional functionality can be introduced.

**Scheme 1**

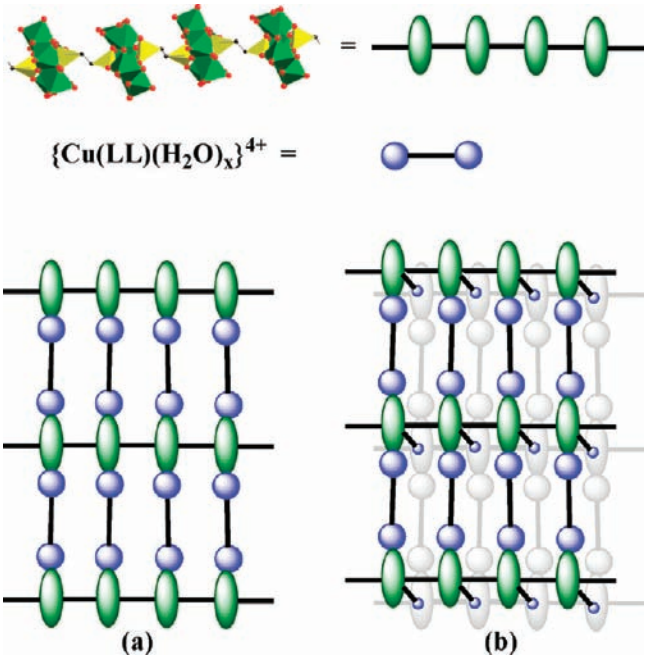


In its most fundamental manifestation, the oxomolybdate−organodiphosphonate system provides one-dimensional structures of the type $\{Mo_5O_{15}(O_3P\text{-tether-}PO_3)\text{-}MoO_{15}\text{-}\}_n^{4n-}$. Charge compensation can be provided by simple secondary metal−organic groups such as $\{Cu(bpy)_2\}^{2+}$ (bpy = bipyridine), containing coordinatively unsaturated oxophilic metal sites that coordinate to surface oxo groups of the oxomolybdate cluster. Of course, if a binucleating ligand is introduced, such as tetrapyridylpyridine (tpypr), the $\{Cu_2(tpypr)\}^{4+}$ unit can bridge oxomolybdate−organodiphosphonate chains to expand the dimensionality of the structure.

The identity of the binucleating ligand is one of several structural determinants for materials of the general class of metal-binucleating ligand/oxomolybdenum-diphosphonate $\{M_2(LL)\}^{n+}/Mo_xO_y\{H_zO_3P\text{-tether-}PO_3H_z\}^{m-}$. Other factors include the size of the molybdate clusters and consequently the number of potential linkage sites on the oxide surface, the coordination preferences of the secondary metal, and the diphosphonate tether length and identity. With respect to the secondary metal-binucleating ligand subunit $\{M_2(LL)\}^{n+}$, we have focused on Cu(II), Ni(II), and Co(II) with tetrapyridylpyrazine (Scheme 1). Copper(II) has proved the most versatile secondary metal because of its structural flexibility in adopting Jahn−Tellar distorted "4 + 1" and "4 + 2" geometries. Since the complex structures of the materials of the Cu(II)-tpyprz/$Mo_xO_y$-diphosphonate family generally derive from the linking of $\{Mo_5O_{15}(O_3PR)_2\}_n^{4n-}$ chains through $\{Cu_2(tpyprz)\}^{4+}$ rods, the structural consequences

(21) Special thematic issue on polyoxometalates: Hill, C. L. *Chem. Rev.* **1998**, *98*, 1−387.
(22) *Polyoxometalate Chemistry: From Topology Via Self-Assembly to Applications*; Pope, M. T., Muller, A., Eds.; Kluwer Academic: Dordrecht, The Netherlands, 2001.
(23) Pope, M. T. *Heteropoly and Isopoly Oxometalates*; Springer: Berlin, 1983.
(24) *Polyoxometalates: From Platonic Solids to Anti-Retroviral Activity*; Pope, M. T., Muller, A., Eds.; Kluwer Academic: Dordrecht, The Netherlands, 1994.
(25) Jolivet, J.-P. *Metal Oxide Chemistry and Synthesis: From Solution to Solid State*, John Wiley: New York, 2000.
(26) Katnoulis, D. E. *Chem. Rev.* **1998**, *98*, 359.
(27) Xu, Y.; Xu, J. Q.; Zhang, K. L.; Zhang, Y.; You, X. Z. *Chem. Commun.* **2000**, 153.
(28) Nyman, N.; Bonhomme, F.; Alam, T. M.; Rodriguez, A. M.; Cherry, B. R.; Krumhansl, J. L.; Nenoff, T. M.; Sattler, A. M. *Science* **2002**, *297*, 996.
(29) Ritchie, C.; Burkholder, E.; Kögerler, P.; Cronin, L. *Dalton Trans.* **2006**, 1712.
(30) Devi, R. N.; Burkholder, E.; Zubieta, J. *Inorg. Chim. Acta* **2003**, *348*, 150.
(31) Zheng, P. Q.; Ren, Y. P.; Long, L. S.; Huang, R. B.; Zheng, L. S. *Inorg. Chem.* **2005**, *44*, 1190.
(32) An, H. Y.; Li, Y. G.; Xiao, D. R.; Wang, E. B.; Sun, C. Y. *Cryst. Growth Des.* **2006**, *6*, 1107.
(33) Cao, R. G.; Liu, S. X.; Xie, L. H.; Pan, Y. B.; Cao, J. F.; Ren, Y. H.; Xu, L. *Inorg. Chem.* **2007**, *46*, 3541.
(34) Wu, C. D.; Lu, C. Z.; Zhuang, H. H.; Huang, J. S. *J. Am. Chem. Soc.* **2002**, *124*, 3836.
(35) Lu, Y.; Xu, Y.; Li, Y.G.; Wang, E. B.; Xu, X. X.; Ma, Y. *Inorg. Chem.* **2006**, *45*, 2055.
(36) Niu, J. Y.; Guo, D. J.; Zhao, J. W.; Wang, J. P. *New J. Chem.* **2004**, *28*, 980.
(37) Yan, B. B.; Xu, Y.; Bu, X. H.; Goh, N.; Chia, L. S.; Stucky, G. D. *J. Chem. Soc., Dalton Trans.* **2001**, 2009.
(38) Finn, R. C.; Zubieta, J. *Inorg. Chem.* **2001**, *40*, 2466.
(39) Burkholder, E.; Zubieta, J. *Chem. Commun.* **2001**, 2056–2057.
(40) Finn, R. C.; Burkholder, E.; Zubieta, J. *Chem. Commun.* **2001**, 1852–1853.
(41) Finn, R. C.; Rarig, R. S.; Zubieta, J. *Inorg. Chem.* **2002**, *41*, 2109.
(42) Burkholder, E.; Wright, S.; Golub, V.; O'Connor, C. J.; Zubieta, J. *Inorg. Chem.* **2003**, *42*, 7460–7471.
(43) Burkholder, E.; Golub, V.; O'Connor, C. J.; Zubieta, J. *Inorg. Chem.* **2003**, *42*, 6729–6740.
(44) Burkholder, E.; Golub, V.; O'Connor, C. J.; Zubieta, J. *Chem. Commun.* **2003**, 2128–2129.
(45) Burkholder, E.; Golub, V.; O'Connor, C. J.; Zubieta, J. *Inorg. Chem.* **2004**, *43*, 7014.
(46) Armatas, N. G.; Allis, D. G.; Prosvirin, A.; Carnutu, G.; O'Connor, C. J.; Dunbar, K.; Zubieta, J. *Inorg. Chem.* **2008**, *47*, 832.
(47) Kwak, W.; Pope, M. T.; Scully, T. F. *J. Am. Chem. Soc.* **1975**, *97*, 5735.
(48) Hedman, B. *Acta Crystallogr.* **1980**, *B36*, 2241.
(49) Kwak, W.; Rajkovic, L. M.; Stalick, J. K.; Pope, M. T.; Quicksall, C. O. *Inorg. Chem.* **1976**, *15*, 2778.
(50) Vioux, A.; LeBideau, J.; Mutin, P. H.; Leclercq, D. *Top. Curr. Chem.* **2004**, *232*, 145.
(51) Clearfield, A. *Curr. Opin. Solid State Mater. Sci.* **2002**, *6*, 495.
(52) Clearfield, A. *Prog. Inorg. Chem.* **1998**, *47*, 371.
(53) Alberti, G. In *Comprehensive Supramolecular Chemistry*; Atwood, J. L., Davies, J. E. D., Vogel, F., Eds.; Pergamon Press: New York, 1966; Vol. *9*, p 152.
(54) Clearfield, A. In *Comprehensive Supramolecular Chemistry*; Atwood, J. L., Davies, J. E. D., Vogel, F., Eds.; Pergamon Press: New York, 1966; vol. *9*, p 107.
(55) Clearfield, A. *Chem. Mater.* **1998**, *10*, 2801.
(56) Vermeulen, L. A. *Prog. Inorg. Chem.* **1997**, *44*, 143.

**Scheme 2**

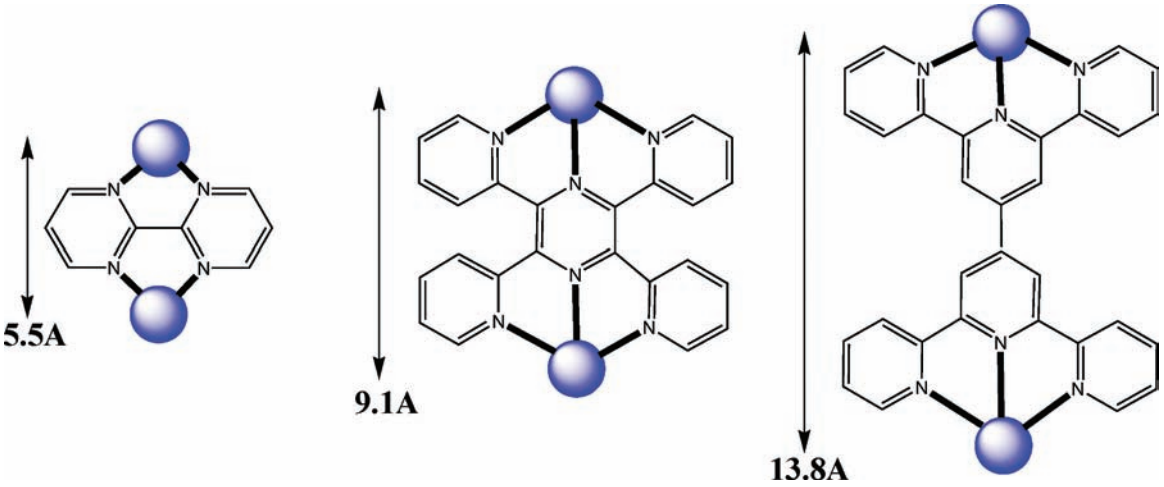


of modifying the secondary metal-binucleating ligand building unit arose quite naturally (Scheme 2). We have addressed the issue in part in studies with Ni(II) and Co(II) as the secondary metal. A natural evolution of the chemistry would focus on the dimensions of the binucleating ligand, most specifically the distance between metal sites. This goal can be readily achieved by expanding the distance between the ligand donor groups, as for bis-terpyridine and analogous phenyl-bridged ligands, and by shortening the distance as in bipyrimidine. In this study of the structural consequences of replacing tetrapyridylpyrazine with bipyrimidine, the syntheses, structures, and magnetic properties of members of the Cu(II)-bpyr/$Mo_xO_y$-diphosphonate family are reported: [{Cu(bpyr)}$_2$$Mo_5O_{15}${$O_3P(CH_3)$}$_2$]·2.5$H_2O$ (**1**·2.5$H_2O$), [{$Cu_2$(bpyr)($H_2O$)$_2$}$Mo_5O_{15}${$O_3P(CH_2CH_3)$}$_2$] (**2**), [{$Cu_2$(bpyr)}$MoO_2${$O_3P(CH_2)PO_3$}$_2$]·2$H_2O$ (**3**·2$H_2O$), [{$Cu_4$(bpyr)$_3$($H_2O$)$_6$}($Mo_5O_{15}$)$_2${$O_3P(CH_2)_2PO_3$}$_2$]·4$H_2O$ (**4**·4$H_2O$), [{$Cu_2$(bpyr)($H_2O$)$_4$}$Mo_5O_{15}${$O_3P(CH_2)_3PO_3$}]·3$H_2O$ (**5**·3$H_2O$), [{$Cu_2$(bpyr)($H_2O$)$_4$}$Mo_5O_{15}${$O_3P(CH_2)_4PO_3$}]·4$H_2O$ (**7**·4$H_2O$), [{$Cu_2$(bpyr)($H_2O$)$_4$} $Mo_5O_{15}${$O_3P(CH_2)_5PO_3$}]·3$H_2O$ (**8**·3$H_2O$), and [{$Cu_2$(bpyr)($H_2O$)$_2$}$Mo_5O_{15}${$O_3P(CH_2)_6PO_3$}] (**9**). The structure and magnetism of the Ni(II) analogue of **5**·3$H_2O$, [{$Ni_2$(bpyr)($H_2O$)$_4$}$Mo_5O_{15}${$O_3P(CH_2)_3PO_3$}]·9$H_2O$ (**6**·9$H_2O$), are also reported for the sake of comparison.

## Experimental Section

**Materials and General Procedures.** Chemicals were used as obtained without further purification, with the exception of the diphosphonic acids ($n$ = 2−6), which were synthesized by slight modification of the reported methods.[57−59] 2,2′-Bipyrimidine (bpyr) was synthesized using the literature method;[60] copper(II) acetate hydrate, hydrofluoric acid, 99.5% molybdenum(VI) oxide, and methylenediphosphonic acid were purchased from Alfa Aesar. All syntheses were carried out in 23 mL of poly(tetrafluoroethylene)-lined stainless steel containers under autogenous pressure. The reactants were stirred briefly, and the initial pH was measured before heating. Water was distilled above 3.0 MΩ in-housing using a Barnstead model 525 Biopure distilled water center. The initial and final pH of each reaction were measured using color pHast sticks. Infrared spectra were obtained on a Perkin-Elmer 1600 series FTIR spectrometer.

**Synthesis of [{Cu(bpyr)}$_2$$Mo_5O_{15}${$O_3P(CH_3)$}$_2$]·2.5$H_2O$ (1·2.5$H_2O$).** A mixture of $MoO_3$ (0.195 g, 1.355 mmol), Cu($CH_3CO_2$)$_2$ (0.085 g, 0.426 mmol), bpyr (0.035 g, 0.221 mmol), $H_3O_3P(CH_3)$ (0.120 g, 1.25 mmol), and $H_2O$ (10g, 555 mmol), in the molar ratio 6.1:1.9:1.0:5.7:2511, to which concentrated $CH_3COOH$ (0.125 g, 2.08 mmol) was added, was stirred briefly before heating to 120 °C for 72 h. Blue platelike crystals of **1**·2.5$H_2O$ were isolated in 66% yield (initial pH, 2; final pH, 2.5). IR (KBr pellet, $cm^{-1}$): 1622(w), 1590(m), 1565(m), 1417(m), 1225(w), 1148(w), 1115(w), 1033(w), 931(s), 890(s), 837(s), 776(m), 727(s), 686(s), 600(s,b), 539(m), 494(w), 478(w), 408(w). Anal. Calcd for $C_{18}H_{23}Cu_2Mo_5N_8O_{23.5}P_2$: C, 15.6; H, 1.67; N, 8.07. Found: C, 15.7; H. 1.45; N, 8.20.

**Synthesis of [{Cu$_2$(bpyr)(H$_2$O)$_2$}Mo$_5$O$_{15}${O$_3$P(CH$_2$CH$_3$)}$_2$] (2).** A solution of $MoO_3$, (0.195 g, 1.35 mmol), Cu($CH_3CO_2$)$_2$ (0.085 g, 0.426 mmol), bpyr (0.035 g, 0.221 mmol), $H_2PO_3(CH_2CH_3)$ (0.090 g, 0.818 mmol), and $H_2O$ (10 g, 555 mmol), in the molar ratio 6.1:1.9:1.0:3.7:2511, to which concentrated HF (50% aqueous, 0.125 g, 3.29 mmol) was added, was stirred briefly before heating to 120 °C for 72 h (initial pH, 2; final pH, 2.5). Green blocks of **2**, suitable for X-ray studies, were isolated in 72% yield. IR (KBr pellet, $cm^{-1}$): 1621(w), 1593(w), 1577(m), 1560(m), 1458(w), 1413(s), 1278(w), 1230(w), 1086(m), 1042(m), 993(m), 939(s), 886(s,b), 833(m), 686(s,b) 612(m), 482(m). Anal. Calcd for $C_6H_{10}CuMo_{2.5}N_2O_{11.5}P$: C, 12.6; H, 1.75; N, 4.89. Found: C, 12.7; H, 1.83; N, 5.11.

**Synthesis of [{Cu$_2$(bpyr)}Mo$_2${O$_3$PCH$_2$PO$_3$}$_2$]·2H$_2$O (3·2H$_2$O).** A mixture of $MoO_3$ (0.195 g, 1.35 mmol), Cu($CH_3CO_2$)$_2$ (0.085 g, 0.426 mmol), bpyr (0.035 g, 0.221 mmol), $H_2PO_3(CH_2)PO_3H_2$ (0.121 g, 0.688 mmol), and $H_2O$ (10 g, 555 mmol), in the molar ratio 6.1:1.9:1.0:3.1:2511, to which concentrated HF (50% aqueous, 0.125 g, 3.29 mmol) was added, was stirred briefly before heating to 120 °C for 72 h. Blue plates of **3** were isolated in 62% yield (initial pH, 1; final pH, 2). IR (KBr pellet, $cm^{-1}$): 3068(s), 2925(s), 1634(w), 1597(s), 1556(m), 1417(s), 1368(m), 1184(s,br), 1066(s,br), 955(s), 931(s), 894(s), 808(m), 747(m), 690(m), 559(m), 526(w), 489(w). Anal. Calcd for $C_{10}H_{14}Cu_2MoN_4O_{16}P_4$: C, 15.1; H, 1.77; N, 7.06. Found: C, 14.6; H, 1.62; N, 7.21.

**Synthesis of [{Cu$_4$(bpyr)$_3$(H$_2$O)$_6$}(Mo$_5$O$_{15}$)$_2${O$_3$P(CH$_2$)$_2$PO$_3$}$_2$]·4H$_2$O (4·4H$_2$O).** The reaction of $MoO_3$ (0.159 g, 1.10 mmol), Cu($CH_3CO_2$)$_2$ (0.088 g, 0.441 mmol), bpyr (0.035 g, 0.221 mmol), $H_2PO_3(CH_2)_2PO_3H_2$ (0.084 g, 0.442 mmol), and $H_2O$ (10 g, 555 mmol), in the molar ratio 5.0:2.0:1.0:2.0:2511, with the addition of concentrated HF (50% aqueous, 0.125 g,

(57) McKenna, C. E.; Higa, M. T.; Cheung, N. H.; McKenna, M. C. *Tetrahedron Lett*. **1977**, 155–8.
(58) Wang, Z.; Heising, J. M.; Clearfield, A. *J. Am. Chem. Soc*. **2003**, *125*, 10375–10383.
(59) Arnold, D. I.; Ouyang, X.; Clearfield, A. *Chem. Mater*. **2002**, *14*, 2020–2027.
(60) Horvath, I. T.; Vlad, G. *J. Org. Chem*. **2002**, *67*, 6550–6552.

3.29 mmol), at 120 °C for 96 h gave blue rod-shaped crystals of $4\cdot 2H_2O$ in 75% yield (initial pH, 1.0; final pH, 2.0). IR (KBr pellet, $cm^{-1}$): 3407(s,br), 3051(s), 2925(s), 1621(w), 1581(m), 1556(w), 1413(m), 1193(w), 1127(m), 1102(m), 1041(w), 1017(w), 910(s,br), 882(m), 853(m), 678(s,br), 575(w), 555(w), 490(w). Anal. Calcd for $C_{14}H_{23}Cu_2Mo_5N_6O_{26}P_2$: C, 12.4; H, 1.70; N, 6.18. Found: C, 12.6; H, 1.83; N, 6.01.

**Synthesis of $[\{Cu_2(bpyr)(H_2O)_4\}Mo_5O_{15}\{O_3P(CH_2)_3PO_3\}]\cdot 3H_2O$ ($5\cdot 3H_2O$).** A solution of $MoO_3$ (0.159 g, 1.10 mmol), $Cu(CH_3CO_2)_2$ (0.088 g, 0.441 mmol), bpyr (0.035 g, 0.221 mmol), $H_2PO_3(CH_2)_3PO_3H_2$ (0.090 g, 0.441 mmol), and $H_2O$ (10 g, 555 mmol), in the molar ratio 5.0:2.0:1.0:2.0:2511, in the presence of concentrated HF (50% aqueous, 0.125 g, 3.29 mmol), was heated at 120 °C for 96 h to give blue crystals of $5\cdot 3H_2O$. These were isolated in 72% yield as crystals suitable for X-ray diffraction (initial pH, 2.0; final pH, 3.0). IR (KBr pellet, $cm^{-1}$): 3444(s,br), 3080(s), 2921(s), 2856(s), 1736(w), 1712(w), 1699(w), 1625(w), 1585(s), 1560(w), 1417(s), 1225(w), 1197(w), 1111(m), 1033(m), 968(s), 927(s), 898(s), 788(w), 682(s,br), 572(w). Anal. Calcd for $C_{11}H_{26}Cu_2Mo_5N_4O_{28}P_2$: C, 9.93; H, 1.97; N, 4.21. Found: C, 9.75; H, 2.11; N, 4.12.

**Synthesis of $[\{Ni_2(bpyr)(H_2O)_4\}Mo_5O_{15}\{O_3P(CH_2)_3PO_3\}]\cdot 9H_2O$ ($6\cdot 9H_2O$).** The reaction of $MoO_3$ (0.160 g, 1.112 mmol), $Ni(CH_3CO_2)_2\cdot 4H_2O$ (0.110 g, 0.442 mmol), bpyr (0.035 g, 0.221 mmol), $H_2O_3P(CH_2)_3PO_3H_2$ (0.084 g, 0.442 mmol), $H_2O$ (10.03 g, 557 mmol), and HF (50% aqueous, 0.125 g, 3.29 mmol) in the molar ratio 5.03:2.00:1.00:2.00:2520:13.89 at 160° C for 96 h provided orange crystals of $6\cdot 9H_2O$ in 35% yield on the basis of Mo. While most of the crystals were intergrown, several which were suitable for single-crystal X-ray diffraction were identified (initial pH, 1.5; final pH, 1.0). IR (KBr pellet, $cm^{-1}$): 3420(s), 1700(w), 1632(w), 1595(w), 1480(w), 1410(m), 1315(w), 1200(w), 1129(m), 1050(m), 1035(m), 940(m), 915(s), 895(s), 770(m), 700(s), 560(m), 535(m). Anal. Calcd for $C_{11}H_{38}Mo_5N_4Ni_2O_{34}P_2$: C, 9.23; H, 2.66; N, 3.92. Found: C, 9.44; H, 2.75; N, 3.81.

**Synthesis of $[\{Cu_2(bpyr)(H_2O)_4\}Mo_5O_{15}\{O_3P(CH_2)_4PO_3\}]\cdot 4H_2O$ ($7\cdot 4H_2O$).** A solution of $MoO_3$ (0.195 g, 1.35 mmol), $Cu(CH_3CO_2)_2$ (0.085 g, 0.426 mmol), bpyr (0.035 g, 0.221 mmol), $H_2PO_3(CH_2)_4PO_3H_2$ (0.095 g, 0.436 mmol), and $H_2O$ (10 g, 555 mmol), in the molar ratio 6.1:1.9:1.0:2.0:2511, in the presence of concentrated HF (50% aqueous, 0.125 g, 3.29 mmol), was stirred briefly before heating to 120 °C for 96 h. Blue crystals of $7\cdot 4H_2O$, suitable for X-ray diffraction, were isolated in 62% yield (initial pH, 2.0; final pH, 2.5). IR (KBr pellet, $cm^{-1}$): 3485(s,br), 3415(s,br), 3080(s), 3002(s), 1622(m), 1593(m), 1560(w), 1454(w), 1417(s), 1328(w), 1295(w), 1225(w), 1197(w), 1176(w), 1111(m), 1099(m), 1074(m), 1037(m), 980(m), 923(s), 845(m), 694(s,br), 592(w), 572(w), 531(w). Anal. Calcd for $C_{12}H_{30}Cu_2Mo_5N_4O_{29}P_2$: C, 10.6; H, 2.22; N, 4.11. Found: C, 10.5; H, 2.08; N, 4.23.

**Synthesis of $[\{Cu_2(bpyr)(H_2O)_4\}Mo_5O_{15}(O_3P(CH_2)_5PO_3\}]\cdot 3H_2O$ ($8\cdot 3H_2O$).** A mixture of $MoO_3$ (0.195 g, 1.35 mmol), $Cu(CH_3CO_2)_2$ (0.085 g, 0.426 mmol), bpyr (0.035 g, 0.221 mmol), $H_2PO_3(CH_2)_5PO_3H_2$ (0.103 g, 0.444 mmol), and $H_2O$ (10 g, 555 mmol), in the molar ratio 6.1:1.9:1.0:2.0:2511, with concentrated HF (50% aqueous, 0.125 g, 3.29 mmol) as a mineralizer, was stirred briefly before heating to 120 °C for 96 h. Blue platelike crystals of $8\cdot 3H_2O$ were isolated in 78% yield (initial pH, 2.0; final pH, 2.5). IR (KBr pellet, $cm^{-1}$): 3403(s,br), 3064(s), 1622(w), 1589(s), 1564(m), 1417(s), 1303(w), 1225(w), 1184(w), 1103(s), 1070(s), 1037(m), 1001(m), 972(w), 923(s,br), 890(s), 845(m), 792(m), 736(w), 681(s,br), 563(w), 518(w), 482(w). Anal. Calcd for $C_{13}H_{30}Cu_2Mo_5N_4O_{28}P_2$: C, 11.5; H, 2.22; N, 4.12. Found: C, 11.2; H, 2.37; N, 4.00.

**Synthesis of $[\{Cu_2(bpyr)(H_2O)_2\}Mo_5O_{15}\{O_3P(CH_2)_6PO_3\}]$ (9).** The reaction of $MoO_3$ (0.195 g, 1.35 mmol), $Cu(CH_3CO_2)_2$ (0.085 g, 0.426 mmol), bpyr (0.035 g, 0.221 mmol), $H_2PO_3(CH_2)_6PO_3H_2$ (0.11 g, 0.447 mmol), and $H_2O$ (10 g, 555 mmol), in the molar ratio 6.1:1.9:1.0:2.0:2511, and concentrated HF (50% aqueous, 0.125 g, 3.29 mmol) as a mineralizer, at 120 °C for 96 h provided brown plates of **9** in 85% yield (initial pH, 2.0; final pH, 3.0). IR (KBr pellet, $cm^{-1}$): 3350(s,br), 3054(s), 2934(s), 1622(w), 1573(m), 1560(m), 1466(w), 1401(m), 1291(w), 1254(w), 1221(w), 1197(w), 1098(s), 1058(s), 988(s), 939(s), 894(s,br), 829(m), 705(s,br), 592 (m), 539(w), 506(w). Anal. Calcd for $C_7H_{11}CuMo_{2.5}N_2O_{11.5}P$: C, 13.1; H, 1.73; N, 4.36. Found: C, 12.5; H, 1.59; N, 4.42.

**X-Ray Crystallography.** Structural measurements for **1**−**9** were performed on a Bruker-AXS SMART-CCD diffractometer at a low temperature (90 K) using graphite-monochromated Mo Kα radiation ($\lambda_{MoK\alpha}$ = 0.71073 Å).[61] The data were corrected for Lorentz and polarization effects and absorption using SADABS.[62] The structures were solved by direct methods. All non-hydrogen atoms were refined anisotropically. After all of the non-hydrogen atoms were located, the models were refined against $F^2$, initially using isotropic and later anisotropic thermal displacement parameters. Hydrogen atoms were introduced in calculated positions and refined isotropically. Neutral atom scattering coefficients and anomalous dispersion corrections were taken from the *International Tables*, volume C. All calculations were performed using SHELXTL crystallographic software packages.[63] Table 1 contains the crystallographic data for structures **1**−**9**.

**Magnetism.** Magnetic susceptibility measurements were carried out on 20−35 mg samples at a magnetic field of 1000 Oe in the 2−300 K temperature range after zero-field cooling using a Quantum Design MPMS SQUID spectrometer. Calibrating and operating procedures have been reported previously.[64]

## Results and Discussion

**Synthesis and Infrared Spectroscopy.** Hydrothermal synthesis, in combination with the use of organic ligands as structure-directing components, has been extensively explored for the preparation of organic−inorganic hybrid materials.[65−72] For this study, the reactions of $MoO_3$, copper(II) acetate, bipyrimidine, the appropriate phosphonic acid, a mineralizer such as acetic acid or HF, and water at temperatures below 160 °C to avoid ligand degradation provided crystalline samples of compounds **1**−**5** and **7**−**9** in modest to good yields. The reported reaction conditions were optimized by varying stoichiometries, the pH, and temperatures and by the addition or exclusion of mineralizers. The reactions were carried out in an acidic pH range (1.0−3.0), a condition that favors formation of the pentamolybdate clusters. Under basic pH conditions, only amorphous mixtures were observed.

(61) *Bruker-AXS SMART Software*, version 5.630; Siemens Analytical X-ray Instruments, Inc.: Madison, WI, 1994.
(62) Sheldrick, G. M. *SADABS: Program for Empirical Absorption Corrections*; University of Göttingen: Göttingen, Germany, 1996.
(63) Sheldrick, G. M. *SHELXTL-Plus: Program for Refinement of Crystal Structures*, version 6.14; Bruker-AXS: Madison, WI, 1996.
(64) Ortiz-Avila, C.Y.; Bhardwaj, C.; Clearfield, A. *Inorg. Chem.* **1994**, *33*, 2499.
(65) Stein, A.; Keller, S. W.; Mallouk *Science* **1993**, *259*, 1558–1564.
(66) Gopalakrishnan, J. *Chem. Mater.* **1995**, *7*, 1265–1275.
(67) Whittinghan, M. S. *Curr. Opin. Solid State Mater. Sci.* **1996**, *1*, 227–232.
(68) Weller, M.; Dann, S. E. *Curr. Opin. Solid State Mater. Sci.* **1998**, *3*, 137–143.
(69) Gopalakrishnan, J.; Bhuvanrh, N. S. P.; Rangan, K. K. *Curr. Opin. Solid State Mater. Sci.* **1996**, *1*, 285–294.
(70) Yoshimura, M.; Suchanek, W.L.; Byrappa, K. *Mater. Res. Soc. Bull.* **2000**, *25*, 17–25.
(71) Fing, S.; Xu, R. *Acc. Chem. Res.* **2001**, *34*, 239–247.
(72) Zubieta, J. *Comp. Coord. Chem. II* **2003**, *1*, 697−709

**Table 1.** Summary of Crystallographic Data for the Structures of [{Cu(bpyr)}$_2$Mo$_5$O$_{15}${O$_3$P(CH$_3$)}$_2$]·2.5H$_2$O (**1**·2.5H$_2$O), [{Cu$_2$(bpyr)(H$_2$O)$_2$}Mo$_5$O$_{15}${O$_3$P(CH$_2$CH$_3$)}$_2$] (**2**), [{Cu$_2$(bpyr)}MoO$_2${O$_3$P(CH$_2$)PO$_3$}$_2$]·2H$_2$O (**3**·2H$_2$O), [{Cu$_4$(bpyr)$_3$(H$_2$O)$_6$}(Mo$_5$O$_{15}$)$_2${O$_3$P(CH$_2$)$_2$PO$_3$}$_2$]·4H$_2$O (**4**·4H$_2$O), [{Cu$_2$(bpyr)(H$_2$O)$_4$}Mo$_5$O$_{15}${O$_3$P(CH$_2$)$_3$PO$_3$}]·3H$_2$O (**5**·3H$_2$O), [{Ni$_2$(bpyr)(H$_2$O)$_4$}Mo$_5$O$_{15}${O$_3$P(CH$_2$)$_3$PO$_3$}]·9H$_2$O (**6**·9H$_2$O), [{Cu$_2$(bpyr)(H$_2$O)$_4$}Mo$_5$O$_{15}${O$_3$P(CH$_2$)$_4$PO$_3$}]·4H$_2$O (**7**·4H$_2$O), [{Cu$_2$(bpyr)(H$_2$O)$_4$}Mo$_5$O$_{15}${O$_3$P(CH$_2$)$_5$PO$_3$}]·3H$_2$O (**8**·3H$_2$O), [{Cu$_2$(bpyr)(H$_2$O)$_2$}Mo$_5$O$_{15}${O$_3$P(CH$_2$)$_6$PO$_3$}] (**9**)

| | **1** | **2** | **3** |
|---|---|---|---|
| empirical formula | $C_{18}H_{23}Cu_2Mo_5N_8O_{23.50}P_2$ | $C_6H_{10}CuMo_{2.50}N_2O_{11.50}P$ | $C_5H_7CuMo_{0.50}N_2O_8P_2$ |
| fw | 1396.16 | 628.52 | 396.58 |
| cryst syst | monoclinic | monoclinic | monoclinic |
| space group | $P2_1/n$ | $C2/c$ | $C2/c$ |
| $a$, Å | 10.2875(10) | 17.289(13) | 10.369(1) |
| $b$, Å | 26.533(3) | 10.084(8) | 12.141(1) |
| $c$, Å | 12.9834(13) | 16.916(13) | 18.211(1) |
| α, deg | 90 | 90 | 90 |
| $\beta$, deg | 95.002(2) | 95.120(10) | 94.071(2) |
| $\gamma$, deg | 90 | 90 | 90 |
| $V$, Å | 3530.4(6) | 2937.5(4) | 2286.8(4) |
| $Z$ | 4 | 8 | 8 |
| $D_{calcd}$, g cm$^{-3}$ | 2.622 | 2.842 | 2.304 |
| $\mu$, mm$^{-1}$ | 30.95 | 36.98 | 27.50 |
| $T$, K | 90(2) | 90(2) | 90(2) |
| $\lambda$, Å | 0.71073 | 0.71073 | 0.71073 |
| $R_1$ (all data) | 0.0542 | 0.0202 | 0.0292 |
| $wR_2$ (all data) | 0.0815 | 0.0442 | 0.0761 |

| | **4** | **5** | **6** |
|---|---|---|---|
| empirical formula | $C_{14}H_{23}Cu_2Mo_5N_6O_{26}P_2$ | $C_{11}H_{26}Cu_2Mo_5N_4O_{28}P_2$ | $C_{11}H_{38}Mo_5N_4Ni_2O_{34}P_2$ |
| fw | 1360.10 | 1331.08 | 1429.51 |
| cryst syst | triclinic | monoclinic | orthorhombic |
| space group | $P\bar{1}$ | $P2_1/c$ | $P2_12_12_1$ |
| $a$, Å | 10.269(7) | 8.485(1) | 8.4849(7) |
| $b$, Å | 12.723(8) | 19.769(3) | 21.033(2) |
| $c$, Å | 14.852(10) | 18.186(3) | 21.331(2) |
| α, deg | 106.880(10) | 90 | 90 |
| $\beta$, deg | 100.841(10) | 100.27(3) | 90 |
| $\gamma$, deg | 109.890(10) | 90 | 90 |
| $V$, Å | 1654.88(19) | 3001.7(7) | 3806.8(5) |
| $Z$ | 2 | 4 | 4 |
| $D_{calcd}$, g cm$^{-3}$ | 2.687 | 2.952 | 2.494 |
| $\mu$, mm$^{-1}$ | 32.99 | 36.40 | 27.63 |
| $T$, K | 90(2) | 90(2) | 90(2) |
| $\lambda$, Å | 0.71073 | 0.71073 | 0.71073 |
| $R_1$ (all data) | 0.0382 | 0.0673 | 0.0725 |
| $wR_2$ (all data) | 0.0773 | 0.0993 | 0.1445 |

| | **7** | **8** | **9** |
|---|---|---|---|
| empirical formula | $C_{12}H_{30}Cu_2Mo_5N_4O_{29}P_2$ | $C_{13}H_{30}Cu_2Mo_5N_4O_{28}P_2$ | $C_7H_{11}CuMo_{2.50}N_2O_{11.50}P$ |
| fw | 1363.12 | 1359.13 | 641.54 |
| cryst syst | monoclinic | monoclinic | monoclinic |
| space group | $P2_1/n$ | $P2_1/n$ | $C2/c$ |
| $a$, Å | 19.315(10) | 10.9953(7) | 17.4298(14) |
| $b$, Å | 9.952(5) | 17.8838(12) | 10.0851(8) |
| $c$, Å | 20.201(10) | 18.5590(12) | 17.4943(14) |
| α, deg | 90 | 90 | 90 |
| $\beta$, deg | 117.502(10) | 93.082(2) | 93.564(2) |
| $\gamma$, deg | 90 | 90 | 90 |
| $V$, Å | 3444.5(3) | 3644.1(14) | 3069.2(4) |
| $Z$ | 4 | 4 | 8 |
| $D_{calcd}$, g cm$^{-3}$ | 2.629 | 2.477 | 2.777 |
| $\mu$, mm$^{-1}$ | 31.77 | 30.01 | 35.42 |
| $T$, K | 90(2) | 90(2) | 90(2) |
| $\lambda$, Å | 0.71073 | 0.71073 | 0.71073 |
| $R_1$ (all data) | 0.0518 | 0.0569 | 0.0406 |
| $wR_2$ (all data) | 0.0773 | 0.1010 | 0.0838 |

[a] $R_1 = \sum|F_o| - |F_c|/\Sigma|F_o|$. $wR_2 = \{\sum[w(F_o^2 - F_c^2)^2]/\sum[w(F_o^2)^2]\}^{1/2}$.

The infrared spectra of the complexes are characterized by two medium-to-strong bands in the 880−940 cm$^{-1}$ range assigned to symmetric and antisymmetric $\upsilon$(Mo = O) of the cis {MoO$_2$} groups of the molybdate units. The medium-to-strong features observed in the 650−770 cm$^{-1}$ region are attributed to $\upsilon$(Mo−O−Mo). A series of three medium-intensity bands in the 960−1200 range are characteristic of the $\upsilon$(P−O) bands of the phosphonate ligands,[72] while the prominent bands in the 1400−1650 cm$^{-1}$ region have been assigned to the bipyrimidine ligand. Compounds **4**−**9** exhibit strong, broad bands in the 3000−3500 cm$^{-1}$ range that are associated with the O−H stretching bands of coordinated water.[73] These features are absent in the spectra of **1**−**3**, which do not exhibit aqua ligation.

**X-Ray Structures.** As anticipated, the structures of this study, with the exception of **3**, are constructed from the common {Mo$_5$O$_{15}$(O$_3$PR)$_2$}$^{4-}$ cluster building block. Charge balance considerations, valence sum calculations on the molybdenum sites,[74] and the magnetic susceptibility studies (vide infra) confirm that the molybdenum sites are exclusively Mo(IV), that is, d$^0$.

As shown in Figure 1, the structure of [{Cu(bpyr)}$_2$Mo$_5$O$_{15}$(O$_3$PCH$_3$)$_2$]·2.5H$_2$O (**1**·2.5H$_2$O) is two-dimensional and constructed from {Cu(bpyr)}$_n^{2n+}$ chains and {Mo$_5$O$_{15}$(O$_3$PCH$_3$)$_2$}$_n^{4n-}$ clusters. The structure of the oxomolybdate-organophosphonate cluster manifests unexceptional features for this well-documented polyoxometalate building block. The cluster consists of a ring of five {MoO$_6$} octahedra linked through four edge-sharing and one corner-sharing interaction. The ring is capped on either face by a tetrahedral {O$_3$PCH$_3$}$^{2-}$ group, each sharing three oxygen vertices with the ring. Two oxygen donors from each phosphorus link the phosphorus site to two molybdenum centers, while the third bridges to a single molybdenum. Each cluster uses terminal oxo groups from three molybdenum sites to link to copper atoms of three adjacent {Cu(bpyr)}$_n^{2n+}$ chains.

The copper-bipyrimidine chains consist of alternating square pyramidal {CuN$_4$O} and octahedral {CuN$_4$O$_2$} sites linked through bis-bidentate bipyrimidine ligands. The copper sites exhibit the common axially distorted geometries associated with the d$^9$ Jahn−Teller influenced geometries. Thus, the octahedral site exhibits equatorial Cu−O and Cu−N distances of 1.933(3) Å (average) and 2.025(5) Å (average), respectively, compared to average axial Cu−O and Cu−N distances of 2.390(3) Å and 2.360(4) Å, respectively. Similarly, for the square pyramidal sites, the basal Cu−O and Cu−N distances are 1.938(2) Å and 2.013(5) Å (average), while the apical Cu−N distance is 2.320(4) Å.

In contrast to the two-dimensional structure of **1**, the ethyl derivative [{Cu$_2$(bpyr)(H$_2$O)$_2$}Mo$_5$O$_{15}$(O$_3$PCH$_2$CH$_3$)$_2$] (**2**) is three-dimensional, as illustrated in Figure 2. The structure is constructed from {Cu$_2$(bpyr)(H$_2$O)$_2$}$^{4+}$ clusters and {Mo$_5$O$_{15}$(O$_3$PCH$_2$CH$_3$)$_2$}$^{4-}$ rings. The molybdophosphonate cluster exhibits the common structural characteristics. Each {Mo$_5$O$_{15}$(O$_3$PCH$_2$CH$_3$)$_2$}$^{4-}$

(73) Poojary, D. M.; Zhang, B.; Bellinghausen, P.; Clearfield, A. *Inorg. Chem.* **1996**, *35*, 4942.
(74) Brown, I. D. In *Structure and Bonding in Crystals*; O'Keefe, M., Navrotsky, A., Eds.; Academic Press: New York, 1981; Vol. *II*.

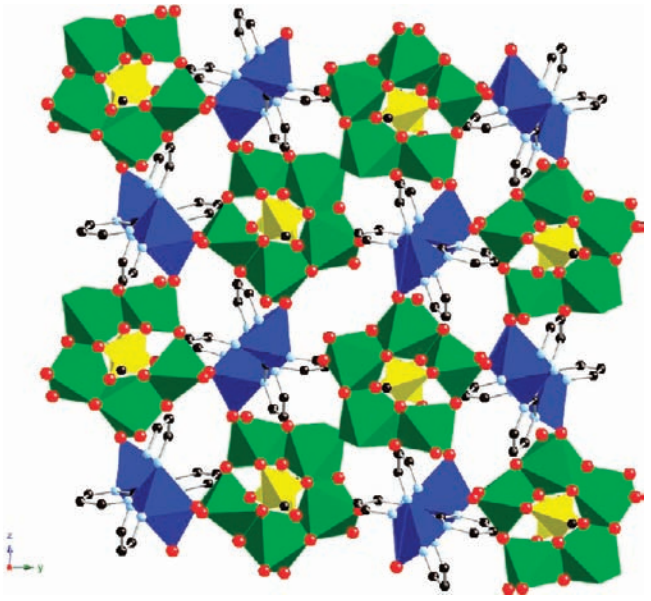

**Figure 1.** A polyhedral view of the structure of $\mathbf{1}\cdot 2.5H_2O$ in the *bc* plane. The water molecules of crystallization have been omitted for clarity. Color scheme: Mo, green polyhedra; Cu, blue polyhedra; P, yellow tetrahedra; O, red spheres; N, light blue spheres; C, black spheres. This color scheme is used throughout.

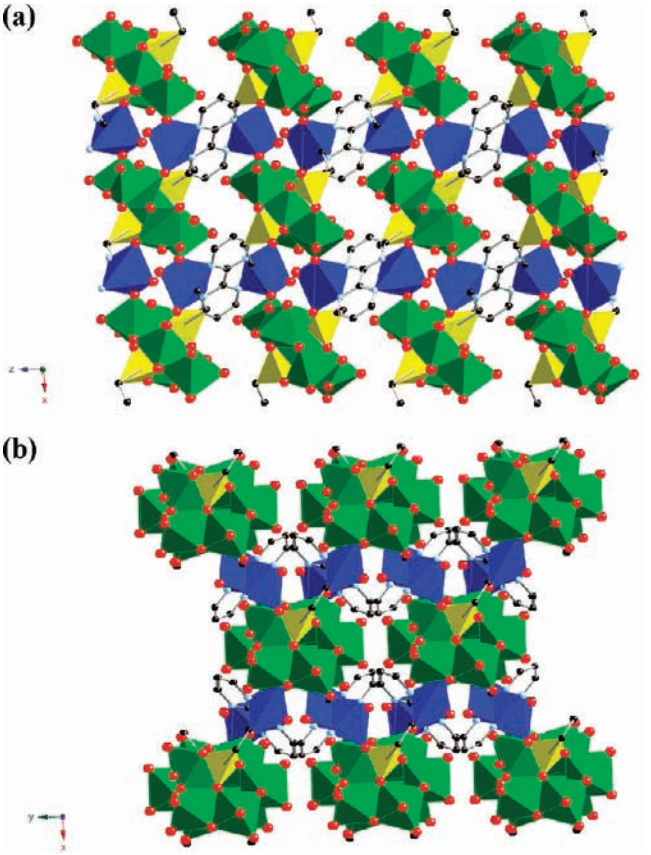


**Figure 2.** (a) A view of the structure of **2** in the *ac* plane. (b) A view of the structure in the *ab* plane.

subunit bonds to four adjacent $\{Cu_2(bpyr)(H_2O)_2\}^{4+}$ groups through two terminal oxo groups and two phosphonate oxygen donors.

The Cu(II) sites exhibit "4 + 1" square pyramidal geometry, with the basal plane defined by an aqua ligand, a terminal oxo group from one phosphomolybdate cluster, a phosphonate oxygen from a second, and a nitrogen donor of the bpyr ligand, while the apical position is occupied by the second bpyr nitrogen donor. Each $\{Cu_2(bpyr)(H_2O)_2\}^{4+}$ subunit links four adjacent phosphomolybdate clusters. Consequently, each $\{Mo_5O_{15}(O_3PCH_2CH_3)_2\}^{4-}$ subunit is tethered to eight adjacent phosphomolybdate clusters through four $\{Cu_2(bpyr)(H_2O)_2\}^{4+}$ rods, to produce a dense three-dimensional framework. The efficient packing of subunits in **2** precludes incorporation of water of crystallization, in contrast to the more open two-dimensional structure of $\mathbf{1}\cdot 2.5H_2O$, which contains 3.2% water by weight.

The first diphosphophosphonate structure, that of $[\{Cu_2(bpyr)\}MoO_2(HO_3PCH_2PO_3)_2]\cdot 2H_2O$ ($\mathbf{3}\cdot 2H_2O$), is also three-dimensional, as shown in Figure 3. Of the series of compounds of this study, phase **3** is the only example which does not exhibit a pentamolybdate building unit, but rather a mononuclear $\{MoO_2(HO_3PCH_2PO_3)_2\}^{4-}$ moiety. The second building block is the common binuclear $\{Cu_2(bpyr)\}^{4+}$ cluster.

The Mo(VI) sites exhibit the *cis*-dioxo unit with the remaining coordination sites occupied by oxygen donors from two chelating methylenediphosphonate ligands. Unlike the α,ω-alkyldiphosphonates, $\{H_xO_3P(CH_2)_nPO_3H_x\}$ where $n \geq 2$, the methylenediphosphonate ligand adopts a chelating modality rather than tethering pentamolybdate clusters. While numerous examples of materials of the $Mo_xO_y$/methylenediphosphonate/M(II)-ligand systems have been described, in no instance does the ligand provide spatial extension between pentanuclear subunits.

The square pyramidal Cu(II) geometry is defined by two bpyr nitrogen donors and two phosphonate oxygen donors in the basal plane and a phosphonate oxygen in the apical position, in contrast to the five coordinate sites of **1** and **2** where the bpyr ligand spans basal/apical sites. Each copper site is associated with oxygen donors from three methylenediphosphonate ligands.

In addition to chelating to the molybdenum center, each diphosphonate ligand bridges to three copper sites, each from a distinct $\{Cu_2(bpyr)\}^{4+}$ subunit. One oxygen site of each ligand is pendant and protonated, projecting into the void space between $\{Cu_2MoO_2(HO_3PCH_2PO_3)_2\}_n$ layers and the buttressing bpyr groups (Figure 3). The water molecules of crystallization also occupy these channels (Supporting Information Figure S4).

The three-dimensional structure of $[\{Cu_4(bpyr)_3(H_2O)_6\}(Mo_5O_{15})_2\{O_3P(CH_2)_2PO_3\}_2]\cdot 4H_2O$ ($\mathbf{4}\cdot 4H_2O$), shown in Figure 4, exhibits the common one-dimensional $[Mo_5O_{15}(O_3P)_2(CH_2)_n\}_n^{4n-}$ chain and an unusual $\{Cu_4(bpyr)_3(H_2O)_6\}^{8+}$ cluster as building blocks. The structure of the phosphomolybdate chain is unexceptional for structures of this type. Each cluster bonds to three copper sites, each from a different chain, through terminal oxo groups.

While a polymeric $\{Cu_2(bpy)\}_n^{2n+}$ subunit was observed for $\mathbf{1}\cdot 2.5H_2O$ and the more common binuclear $\{Cu_2(bpyr)(H_2O)_x\}^{4+}$ building block for **2** and **3**, compound **4** exhibits an intermediate aggregation state for the

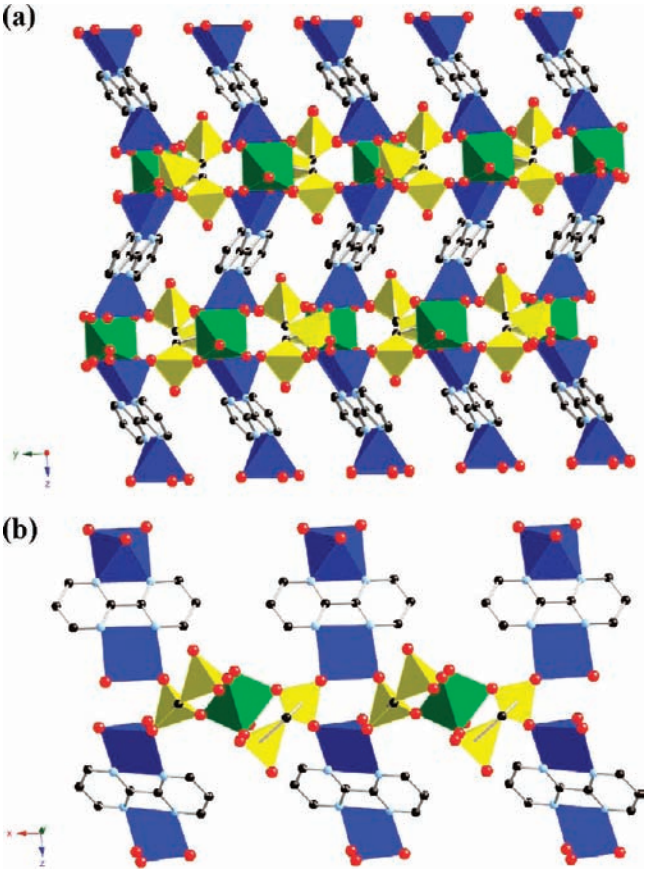


**Figure 3.** (a) A view of the structure of **3** in the *bc* plane. (b) A view of the structural building units in the *ac* plane.

secondary metal−ligand substructure. There are two distinct Cu(II) geometries: the interior pair of copper sites exhibit "4 + 2" distorted octahedral geometry through bonding to two nitrogens from a chelating bpyr ligand, a nitrogen donor from a second bpyr group, and an aqua ligand in the equatorial plane, with the axial positions defined by the second nitrogen donor of the bpyr ligand and a terminal oxo group from a molybdenum site; the exterior pair of copper sites coordinates to the two nitrogen donors of a bpyr ligand and to two terminal oxo groups from two different phosphomolybdate chains in the equatorial plane and two axial aqua ligands. Each copper rod links a phosphomolybdate chain to three adjacent chains, and in this fashion, each chain is linked to six adjacent chains (Figure 4b and Scheme 3).

The three-dimensional structure of $[\{Cu_2(bpyr)(H_2O)_4\}Mo_5O_{15}\{O_3P(CH_2)_3PO_3\}]\cdot 3H_2O$ (**5**$\cdot 3H_2O$) is shown in Figure 5. The framework is constructed from $[Mo_5O_{15}\{O_3P(CH_2)_3PO_3\}]_n^{4n-}$ chains linked through two distinct copper−ligand rods, $\{Cu_2(bpyr)(H_2O)_2\}^{4+}$ and $\{Cu_2(bpyr)(H_2O)_6\}^{4+}$. Each phosphomolybdate cluster of a chain links to four copper sites, two from one binuclear unit and two from two other binuclear rods, through terminal oxo groups. The $\{Cu_2(bpyr)(H_2O)_2\}^{4+}$ subunits link clusters from four adjacent chains, while the $\{Cu_2(bpyr)(H_2O)_6\}^{4+}$ groups link clusters from two adjacent chains.

There are two crystallographically distinct Cu(II) sites, both exhibiting "4+2" axially elongated geometries. For the Cu(1) site, the equatorial plane is defined by the

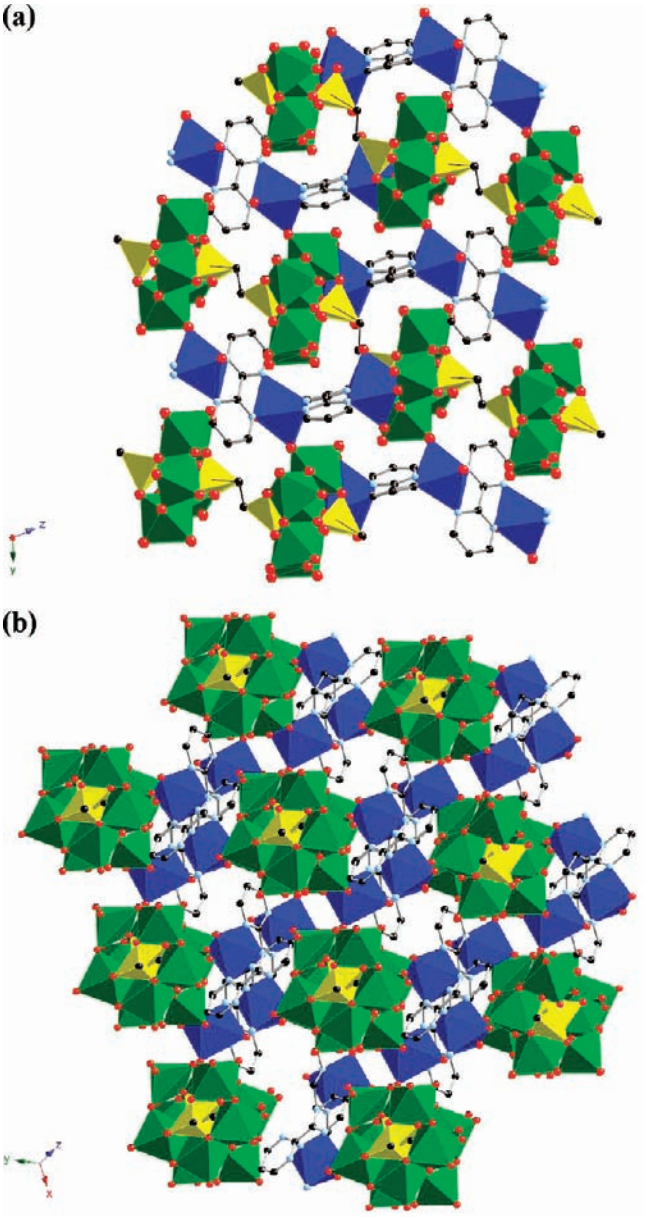


**Figure 4.** (a) Polyhedral view of the structure of **4**$\cdot 4H_2O$ in the *bc* plane. (b) A view of the structure looking down the $\{Mo_5O_{15}(O_3PCH_2CH_2PO_3)\}_n^{4n-}$ chains.

**Scheme 3**

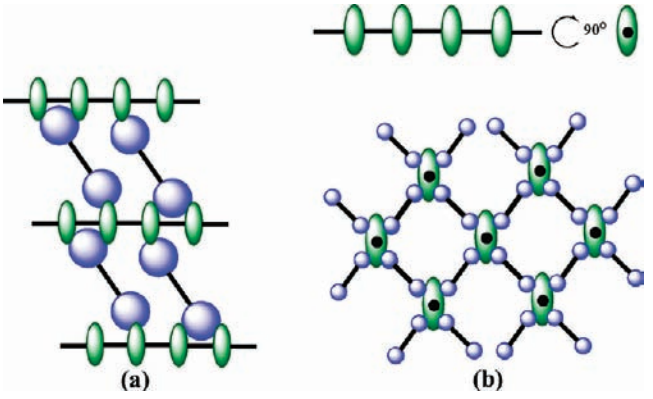


nitrogen donors of the bpyr ligand and two aqua ligands, with an oxo group from a phosphomolybdate cluster and

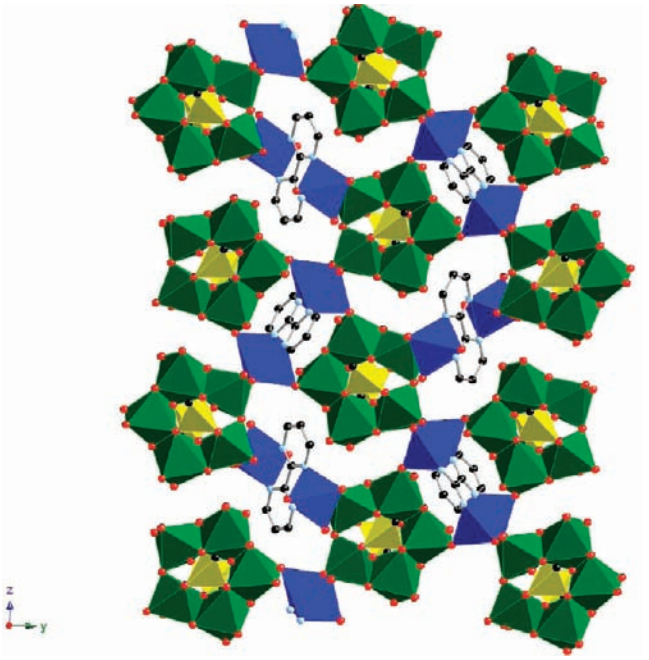

**Figure 5.** A polyhedral view of the structure of $\mathbf{5}\cdot 3H_2O$ viewed parallel to the $\{Mo_5O_{15}(O_3PCH_2CH_2CH_2PO_3)\}_n^{4n-}$ chains (in the *bc* plane).

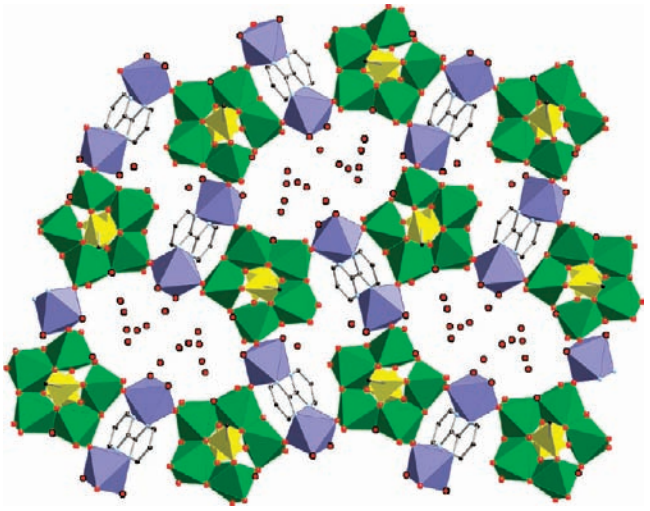

**Figure 6.** A polyhedral view of the structure of $\mathbf{6}\cdot 9H_2O$ in the *bc* plane. The structure is viewed parallel to the $\{Mo_5O_{15}(O_3PCH_2CH_2CH_2PO_3)\}_n^{4n-}$ chain axes to illustrate the large void volume occupied by water of crystallization.

an aqua ligand in the axial positions. For the Cu(2) site, the equatorial plane is occupied by the bpyr nitrogen donors, a cluster oxo group, and an aqua ligand, while two bridging oxo groups define the axial positions.

The water molecules of crystallization reside in narrow galleries between $[\{Cu_2(bpyr)\}Mo_5O_{15}(O_3P\text{-})_2]_n^{4n-}$ layers that run parallel to the *ab* plane (Supporting Information Figure S7). From this perspective, the structure may be described as copper−bipyrimidine/phosphomolybdate layers buttressed by the propylene chains of the diphosphonate ligands.

A Ni(II) material of the same general composition as that of compound **5**, $[\{Ni_2(bpyr)(H_2O)_4\}Mo_5O_{15}\{O_3P(CH_2)_3PO_3\}]\cdot 9H_2O$ ($\mathbf{6}\cdot 9H_2O$), shown in Figure 6,

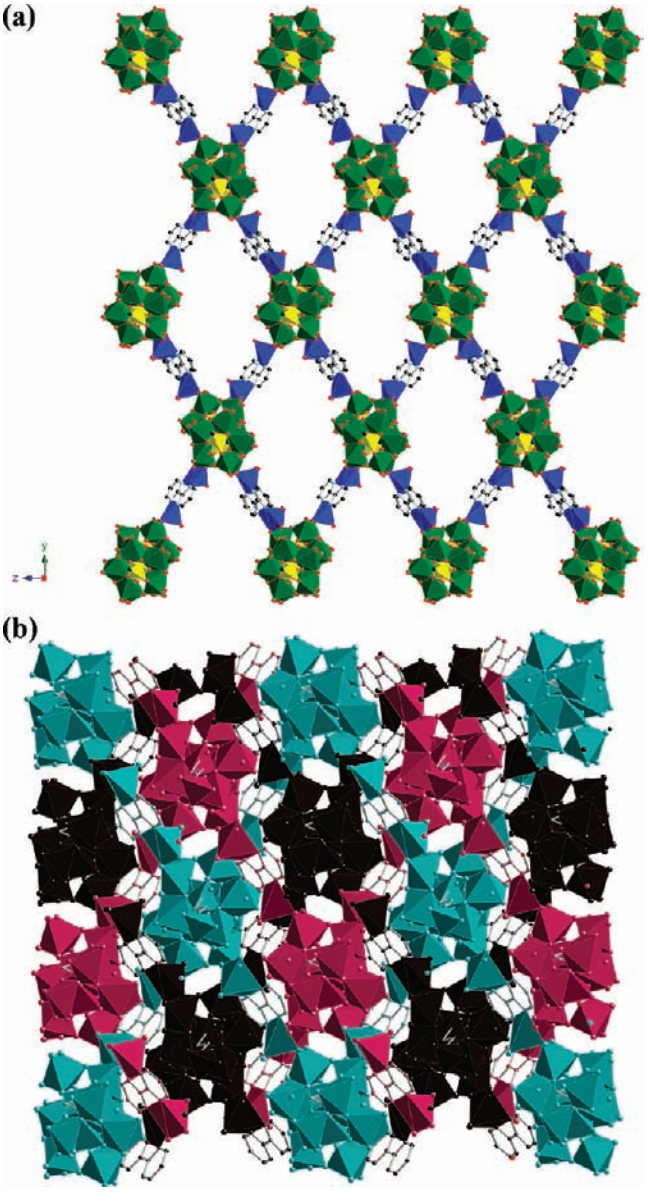


**Figure 7.** (a) A view of a single framework of $\mathbf{7}\cdot 4H_2O$ in the *bc* plane and parallel to the $\{Mo_5O_{15}(O_3PCH_2CH_2CH_2CH_2PO_3)\}_n^{4n-}$ chain axes. (b) A view of the structure showing the three-fold interpenetration of frameworks.

was also prepared. While the structure of **6** exhibits similarities to that of **5**, the detailed connectivity pattern results in a more open framework and consequently considerably more effective entrapment of water of crystallization. Once again, the structure is constructed from $[Mo_5O_{15}\{O_3P(CH_2)_3PO_3\}]_n^{4n-}$ chains linked through $\{Ni_2(bpyr)(H_2O)_4\}^{4+}$ rods. Each phosphomolybdate cluster uses four terminal oxo groups to link to nickel sites from three different nickel−bipyrimidine rods in an analogous fashion to compound **5**. However, in contrast to **5**, compound **6** exhibits a single unique binuclear rod $\{Ni_2(bpyr)(H_2O)_4\}^{4+}$, each of which links clusters from three adjacent chains. The result is an open framework when the structure is viewed parallel to the phosphomolybdate chain axis.

There are two distinct Ni(II) octahedra. Both coordination sites are defined by two bpyr nitrogen donors, two

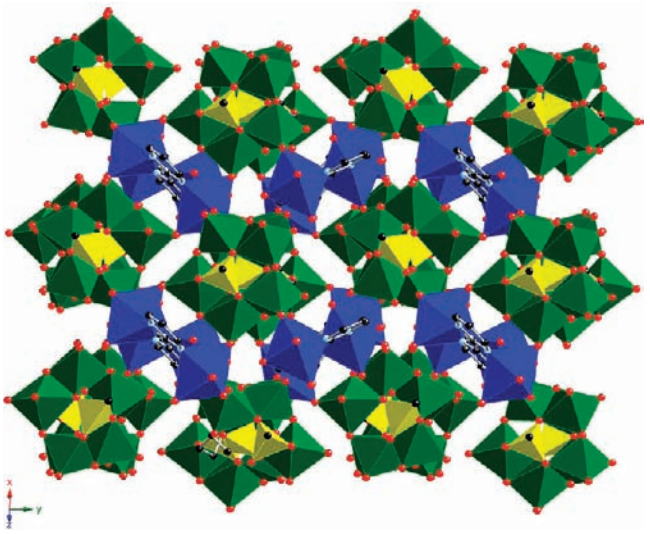

**Figure 8.** The structure of **8**·3$H_2O$ viewed parallel to the $[Mo_5O_{15}\{O_3P(CH_2)_5PO_3\}]_n^{4n-}$ chains.

aqua ligands, and two cluster oxo groups. However, in the Ni(1) site the oxo-groups are mutually *trans*, while for Ni(2) the oxo-groups adopt a *cisoid* configuration.

The three-dimensional structure of the butyldiphosphonate derivative, $[\{Cu_2(bpyr)(H_2O)_4\}Mo_5O_{15}\{O_3P(CH_2)_4PO_3\}]\cdot 4H_2O$ (**7**·4$H_2O$), is also constructed from common building blocks, $[Mo_5O_{15}\{O_3P(CH_2)_4PO_3\}]_n^{4n-}$ chains and $\{Cu_2(bpyr)(H_2O)_4\}^{4+}$ rods (Figure 7). In this instance, each cluster links to two copper−bpyr rods through two terminal oxo groups. As the linkage points alternate from side to side down the chain, each chain is linked to four adjacent chains to give an open-framework profile. However, the structure contains three interpenetrating frameworks, as shown in Figure 7b, to produce a dense framework material. Such interpenetration of two or more independent frameworks is not uncommon for metal organic frameworks (MOFs),[75] although it is relatively unusual for materials of the $Mo_xO_y$/diphosphonate/M(II)-ligand families.

In this case, the copper sites adopt "4 + 1" square pyramidal geometry with the basal plane occupied by the bpyr nitrogen donors, an aqua ligand, and a bridging oxo group from the cluster subunits. An aqua ligand defines the apical position.

The three-dimensional structure of $[\{Cu_2(bpyr)(H_2O)_4\}Mo_5O_{15}\{O_3P(CH_2)_5PO_3\}]\cdot 3H_2O$ (**8**·3$H_2O$) is reminiscent of that of compound **5**. As shown in Figure 8, the structure is constructed from the usual $[Mo_5O_{15}\{O_3P(CH_2)_5PO_3\}]_n^{4n-}$ chains and $\{Cu_2(bpyr)(H_2O)_2\}^{4+}$ and $\{Cu_2(bpyr)(H_2O)_6\}^{4+}$ rods. Each cluster uses four terminal oxo groups to link to four copper sites from three binuclear Cu−bpyr units. The $\{Cu_2(bpyr)(H_2O)_2\}^{4+}$ rods link clusters from two neighboring chains, when the $\{Cu_2(bpyr)(H_2O)_6\}^{4+}$ units link clusters from four chains.

When the structure is viewed parallel to the crystallographic *a* axis, the architecture may be described as $[\{Cu_2(bpyr)\}Mo_5O_{15}(O_3P\text{-})_2]_n^{4n-}$ layers buttressed by the pentyl chains of the diphosphonate ligand, in a fashion similar to that discussed for compound **5** (Supporting Information Figure S11). The only significant difference between these profiles for **5** and **8** is the expansion of the width of the gallery between layers in **8** compared to **5** as a result of the greater spatial extension provided by the expanded tether length of **8** (4.79 Å for **5** vs 7.19 Å for **8**).

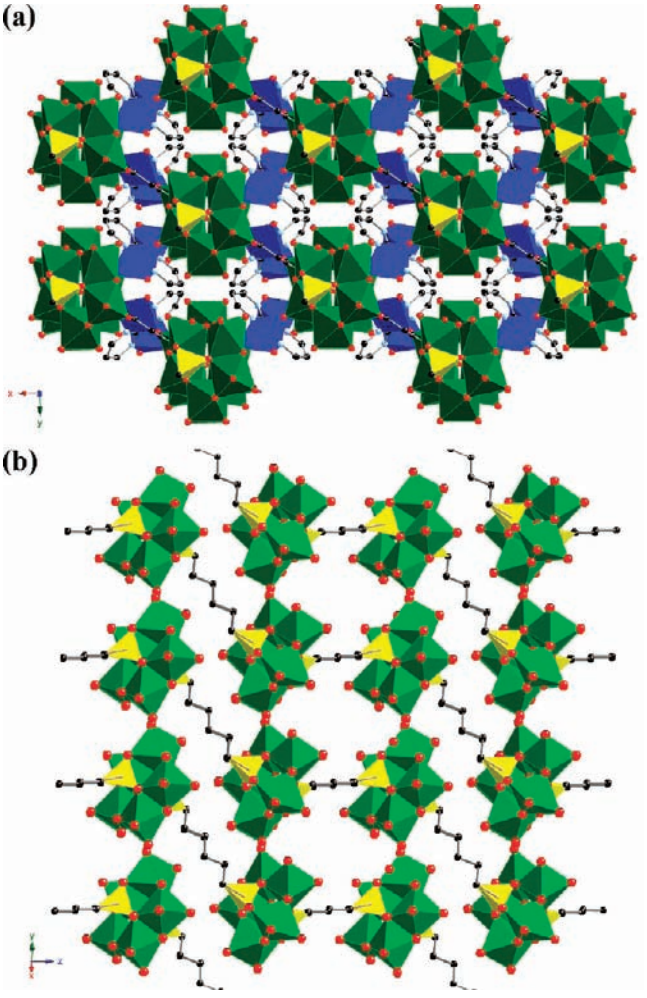

**Figure 9.** (a) The structure of **9** in the *ab* plane, parallel to the $[Mo_5O_{15}\{O_3P(CH_2)_6PO_3\}]_n^{4n-}$ chains. (b) The structure of **9** with the $\{Cu_2(bpyr)(H_2O)_2\}^{4+}$ groups removed to show the building of the $[Mo_5O_{15}\{O_3P(CH_2/_6PO_3\}]_n^{4n-}$ chains.

The recurrent theme of three-dimensional structures is maintained in $[\{Cu_2(bpyr)(H_2O)_2\}Mo_5O_{15}\{O_3P(CH_2)_6PO_3\}]$ (**9**), shown in Figure 9. While the structure exhibits the common building blocks of phosphomolybdate chains and Cu−bpyr rods, a number of notable features emerge in the detailed analysis of the connectivities and geometries. In this case, each phosphomolybdate cluster links to four copper sites from four distinct $\{Cu_2(bpyr)(H_2O)\}^{4+}$ units. However, linkage is achieved through two terminal oxo groups and two phosphonate oxygen donors, one on either face of the molybdate ring. The cluster is somewhat distorted as a consequence of these $\mu_3$-oxygen interactions, resulting in a pronounced buckling of the $[Mo_5O_{15}\{O_3P(CH_2)_6PO_3\}]_n^{4n-}$ chains, as shown in Figure 9b. The structure may be described as $\{Cu_2Mo_5O_{15}(O_3PR)_2\}_n$ layers, buttressed by the alkyl chains of the diphosphonate ligand and the bpyr ligands, when viewed parallel to the *b* axis.

(75) Luo, F.; Zhang, J.-M.; Batten, S. R. *Chem. Comm.* **2007**, 3744.

The Cu(II) sites enjoy "4+1" square pyramidal geometry, with the nitrogen donors of the bpyr ligand spanning basal/apical positions. Each $\{Cu_2(bpyr)(H_2O)_2\}^{4+}$ rod links three adjacent phosphomolybdate chains. In turn, each phosphomolybdate chain is tethered to six adjacent chains to produce a relatively dense framework structure.

**General Structural Observations.** The $\{Mo_5O_{15}(O_3PR)_2\}^{4-}$ cluster is a nearly ubiquitous structural component and appears for all compounds with the exception of the methylenediphosphonate phase, $[\{Cu_2(bpyr)\}MoO_2(HO_3PCH_2PO_3)_2]\cdot 2H_2O$ ($\mathbf{3}\cdot 2H_2O$). The absence of the pentanuclear phosphomolybdate motif for **3** is not unanticipated, as the methylenediphosphonate ligand tends to form six-membered chelate rings {Mo−O−P−C−P−O−} upon coordination to the molybdenum, thus precluding isolation of the prototypical pentanuclear ring structure. This is a persistent observation, previously noted for $[\{Cu_2(tpyprz)(H_2O)\}Mo_3O_8(HO_3PCH_2PO_3)_2]$ and $[\{Cu_2(tpyprz)(H_2O)\}_2(Mo_3O_8)_2(O_3PCH_2PO_3)_3]$ of the $Mo_xO_y$/diphosphonate/Cu-tpyprz family (tpyprz = tetra-2-pyridylpyrazine). It is noteworthy, however, that the latter materials are one-dimensional while **3** is two-dimensional.

The diphosphonate phases with an alkyl tether length greater than 1, compounds **4**−**9** of this study, invariably exhibit the one-dimensional $\{Mo_5O_{15}(O_3P(CH_2)_nPO_3\}_n^{4n-}$ chain as a structural building block. While this is a recurrent theme of the $Mo_xO_y$/diphosphonate/M(II)-ligand family of materials, considerable structural variability arises as a consequence of the interplay of numerous structural determinants. As previously noted, these include the coordination preferences of the secondary metal M(II), the "soft" M−O−P angles, the number and locations of attachment points of the M(II)−ligand unit on the phosphomolybdate clusters, variable aqua coordination to the secondary metal sites, folding of the alkyl chains of the diphosphonate ligands, and variable protonation of the phosphonate oxygen sites. In this instance, the structural influences of the identity of the binucleating ligand LL of the $\{M^{II}_2(LL)\}^{4+}$ component was addressed.

It is instructive to compare the structures of the materials of this study exhibiting the $[Mo_5O_{15}\{O_3P(CH_2)_nPO_3\}]_n^{4n-}$ chain motif, compounds **4**−**9**, with those of the previously reported $[Mo_5O_{15}\{O_3P(CH_2)_nPO_3\}]_n^{4n-}$/M(II)−tpyprz families, where M(II) = Co, Ni, and Cu. Some of the relevant structural information for these materials is summarized in Table 2. It is noteworthy that, whereas the M(II)−tpyprz-based phases exhibit the full range of dimensionalities, 1-D, 2-D, and 3-D, the Cu(II)−bpyr-based materials of this study are exclusively three-dimensional. It is also apparent that the dimensionality of the phase does not correlate either with the number of contact points on the surface of the $\{Mo_5O_{15}(O_3PR)_2\}^{4-}$ cluster building blocks used to link to the M(II) or secondary metal unit, or with the number of phosphomolybdate clusters linked by the M(II)−binucleating ligand components. For example, the three-dimensional structure of $[\{Cu_2(bpyr)(H_2O)_4\}Mo_5O_{15}\{O_3P(CH_2)_4PO_3\}]$ is constructed from phosphomolybdate clusters sharing only two vertices with the $\{Cu_2(bpyr)(H_2O)_4\}^{4+}$ rods, which in turn bridge only two cluster units. In contrast, the structures of $[\{M_4(tpyprz)_3\}\{Mo_5O_{15}(O_3P(CH_2)_2PO_3)\}]$ (M = Co, Ni) exhibit three contact points per cluster with each M(II)−tpyprz subunit bridging four clusters to produce a two-dimensional architecture. As shown in the schematic, the detailed connectivity pattern adopted between the building blocks dictates the overall dimensionality of the material. The two-dimensional network of the schematic is representative of the structure of $[\{Cu_2(tpyprz)(H_2O)_2\}Mo_5O_{15}(O_3PCH_2CH_2PO_3)]$, which exhibits three contact points on each cluster with each $\{Cu_2(tpyprz)(H_2O)_2\}^{4+}$ rod linking three clusters. In contrast, the three-dimensional framework of the schematic represents the connectivity pattern of $[\{Cu_2(bpyr)(H_2O)_4\}Mo_5O_{15}\{O_3P(CH_2)_4PO_3\}]$ where the $\{Cu_2(bpyr)(H_2O)_4\}^{4+}$ units bridge two clusters, each of which contributes two attachments points in a staggered orientation along the chain.

That the Cu(II)−bpyr materials of this study adopt exclusively three-dimensional structures may reflect the reduced steric constraints associated with the bpyr ligand in comparison to tpyprz. This may allow more efficient packing of the phosphomolybdate chains. While the bis-bidentate character of bpyr affords the M(II) sites an additional coordination site in comparison to the bis-tridentate tpyprz, this feature is not reflected in a consistent increase in the number of clusters bridged by $\{M_2(bpyr)\}^{4+}$ units in comparison to $\{M_2(tpyprz)^{4+}$ rods. This observation appears to be related to steric considerations and charge density matching between the anionic chains and cationic rods. As we have noted previously, the phosphomolybdate clusters can contribute a maximum of four contact points based on sterics and charge.

The observation of catenation of Cu(II) sites in compounds **1** and **4** of this study was unexpected. In the family of materials with tpyprz as the ligand to the secondary metal M(II), catenation was observed for several members of the Ni(II) and Co(II) phases, but not for the Cu(II)-containing materials. This observation was rationalized on the basis of the Jahn−Teller distorted geometries (square planar, 4 + 1 square pyramidal, and 4 + 2 distorted octahedral) adopted by Cu(II), which preferentially binds to a single tpyprz $N_3$- terminus in forming $\{Cu_2(tpyprz)(H_2O)_x\}^{4+}$ units with $\{CuN_3O\}$, $\{CuN_3O_2\}$, or $\{CuN_3O_3\}$ coordination. In contrast, Ni(II) and Co(II) exhibit more regular octahedral coordination and can achieve this by bonding to two tpyprz ligands to give $\{MN_6\}$ coordination geometries. The balance between this preference and the oxophilicity of the M(II) cations results in varying degrees of oligomerization. However, since bpyr is bidentate rather than tridentate, the Cu(II) sites can bond to two bpyr ligands and adopt distorted geometries through bonding to one or two oxygen atoms of clusters or aqua ligands to provide 4 + 1 $\{CuN_4O\}$ or 4 + 2 $\{CuN_4O_2\}$ coordination geometries.

The range of phosphomolybdate clusters bridged by a given secondary metal−ligand subunit is reflected in the variability in the number of aqua ligands coordinated to the secondary metal sites. A given M(II) site may be associated with zero to two aqua ligands which serve to complete the coordination sphere. Consequently, structural prediction for these phases is problematic given the somewhat promiscuous incorporation of aqua ligands.

**Thermal Analyses.** The thermogravimetric profile of compound **1** (Supporting Information Figure S13) is

**Table 2.** Summary of Selected Structural Characteristics of Materials of the General Type Catena-$[Mo_5O_{15}\{O_3P(CH_2)_nPO_3\}]_n^{4n-}$/M(II)-Binucleating Ligand ($n \geq 2$)

| compound | overall dimensionality | contact points on $\{Mo_5O_{15}(O_3PR)_2\}^{4-}$ Clusters | number of clusters linked by M(II)-ligand unit | M(II)-binucleating ligand substructure |
|---|---|---|---|---|
| $[\{Cu_2(tpyprz)(H_2O)_2\}Mo_5O_{15}(O_3PCH_2CH_2PO_3)]$ octahedra | 2-D | 3 | 3 | binuclear unit: $\{CuN_3O_2\}$ square pyramid and $\{CuN_3O_3\}$ 4+2 |
| $[\{Ni_4(tpyprz)_3\}\{Mo_5O_{15}(O_3PCH_2CH_2PO_3)\}_2]$ | 2-D | 3 | 4 | tetranuclear unit: 2×$\{NiN_6\}$ and 2×$\{NiN_3O_3\}$ octahedra |
| $[\{Co(H_2tpyprz)\}Mo_5O_{15}(O_3PCH_2CH_2PO_3)]$ octahedra | 1-D | 3 | 2 | mononuclear unit: $\{CoN_3O_3\}$ |
| $[\{Co_4(tpyprz)_3\}\{Mo_5O_{15}(O_3PCH_2CH_2PO_3)\}_2]$ | 2-D | 3 | 4 | Tetranuclear unit: 2x$\{CoN_6\}$ and 2x$\{CoN_3O_3\}$ octahedra |
| $[\{Cu_4(bpyr)_3(H_2O)_6\}\{Mo_5O_{15}(O_3PCH_2CH_2PO_3)\}_2]$ | 3-D | 3 | 4 | tetranuclear unit: 2×$\{CuN_4O_2\}$ 2×$\{CuN_2O_4\}$ octahedra |
| $[\{Cu_2(tpyprz)(H_2O)_2\}Mo_5O_{15}\{O_3P(CH_2)_3PO_3\}]$ | 3-D | 4 | 3 | binuclear unit: $\{CuN_3O_3\}$ 4+2 octahedra |
| $[\{Ni_2(tpyprz)(H_2O)_3\}Mo_5O_{15}\{O_3P(CH_2)_3PO_3\}]$ | 3-D | 3 | 3 | binuclear unit: $\{NiN_3O_3\}$ octahedra |
| $[\{Co_2(tpyprz)(H_2O)_3\}Mo_5O_{15}\{O_3P(CH_2)_3PO_3\}]$ | 3-D | 3 | 3 | binuclear unit: $\{CoN_3O_3\}$ octahedra |
| $[\{Co_2(tpyprz)(H_2O)_3\}Mo_5O_{15}\{O_3P(CH_2)_3PO_3\}]$ | 3-D | 3 | 2 and 3 | binuclear units: $\{CoN_3O(H_2O)_2\}$ and $\{CoN_3O_2(H_2O)\}$ octahedra |
| $[H_3O]_2[\{Co_3(tpyprz)_2(H_2O)_3\}\{Mo_5O_{15}(O_3P(CH_2)_3PO_3)\}_2]$ $\{CoN_3O_3\}$ | 3-D | 1 and 2 | 2 | trinuclear units: $\{CoN_6\}$ and octahedra |

| compound | overall dimensionality | contact points on $\{Mo_5O_{15}(O_3PR)_2\}^{4-}$ clusters | number of clusters linked by M(II)-ligand unit | M(II) binucleating ligand substructure |
|---|---|---|---|---|
| $[\{Cu_2(bpyr)(H_2O)_4\}Mo_5O_{15}\{O_3P(CH_2)_3PO_3\}]$ | 3-D | 4 | 2 and 4 | binuclear units: $\{CuN_2O_3(H_2O)\}$ and $\{CuN_2O(H_2O)_3\}$ octahedra |
| $[\{Ni_2(bpyr)(H_2O)_4\}Mo_5O_{15}\{O_3P(CH_2)_3PO_3\}]$ | 3-D | 4 | 3 | binuclear units: $\{NiN_2O_2(H_2O)_2\}$ octahedra |
| $[\{Cu_2(tpyprz)(H_2O)_2\}Mo_5O_{15}\{O_3P(CH_2)_4PO_3\}]$ octahedra | 3-D | 4 | 3 | binuclear unit: $\{CuN_3O_3\}$ 4+2 |
| $[\{Ni_2(tpyprz)_2\}Mo_5O_{15}\{O_3P(CH_2)_4PO_3\}]$ $\{NiN_3O_3\}$ | 1-D | 3 | 2 | binuclear unit: $\{NiN_6\}$ and octahedra |
| $[\{Ni_2(tpyprz)(H_2O)_2\}Mo_5O_{15}\{O_3P(CH_2)_4PO_3\}]$ octahedra | 3-D | 3 | 4 | binuclear unit: $\{NiN_3O_3\}$ |
| $[\{Co_2(tpyprz)(H_2O)_2\}Mo_5O_{15}\{O_3P(CH_2)_4PO_3\}]$ octahedra | 3-D | 4 | 4 | binuclear unit: $\{CoN_3O_3\}$ |
| $[\{Cu_2(bpyr)(H_2O)_4\}Mo_5O_{15}\{O_3P(CH_2)_4PO_3\}]$ | 3-D | 2 | 2 | binuclear unit: $\{CuN_2O_3\}$ square pyramids |
| $[\{Ni_2(tpyprz)_2\}Mo_5O_{15}\{O_3P(CH_2)_5PO_3\}]$ $\{NiN_3O_3\}$ | 1-D | 3 | 2 | binuclear unit: $\{NiN_6\}$ ad octahedra |
| $[\{Co_2(tpyprz)(H_2O)_3\}Mo_5O_{15}\{O_3P(CH_2)_5PO_3\}]$ octahedra | 3-D | 3 | 3 | binuclear unit: $\{CoN_3O_3\}$ |
| $[\{Cu_2(bpyr)(H_2O)_4\}Mo_5O_{15}\{O_3P(CH_2)_5PO_3\}]$ $\{CuN_2O_2(H_2O)_2\}$ | 3-D | 4 | 2 and 4 | binuclear units: $\{CuN_2O(H_2O)_3\}$ 4+2 octahedra |
| $[\{Cu_2(bpyr)(H_2O)_2\}Mo_5O_{15}\{O_3P(CH_2)_6PO_3\}]$ square | 3-D | 4 | 3 | binuclear units: $\{CuN_3O_3\}$ pyramids |

generally characteristic of the patterns displayed by the hydrates of this study. There is a gradual loss of the water of crystallization between room temperature and 200 °C (2.6% theoretical, ca. 3.0% observed), followed by a gradual weight loss of an additional 7% between 200 °C and 560 °C attributed to partial degradation of the organic ligands. There is a rapid loss of ca. 30% by weight between 560 and 650 °C, corresponding to the decomposition of the bipyrimidine ligands, to give an amorphous gray powder. This pattern of a gradual weight loss, followed by a second, more rapid decomposition is observed for compounds **2**, **3**, **5**, **7**−**9**; however, the onset of the sharp weight loss varies between 560 and 750 °C (Supporting Information Figures S14, S16, S21 S27, S30, and S32).

Compound **4** is somewhat anomalous in that there is a sharp weight loss of 5% between 100 and 130 °C, corresponding to a loss of the water of crystallization (Figure 10a). This dehydration step is followed by a plateau of stability to 350 °C, whereupon there is a 23% weight loss between 350 and 700 °C, associated with the loss of the organic groups and the aqua ligands.

The thermal diffraction profile for **4** (Figure 10b) shows that there is a considerable loss of crystallinity concomitant with the dehydration process. Some crystalline phase persists to ca. 300 °C, whereupon the material becomes amorphous.

The Ni(II) material **6**·9$H_2O$ provides behavior similar to that of **4**. The thermogravimetric analysis (TGA) shows a dehydration process (Supporting Information Figure S24) in the temperature range 40−150 °C with a weight loss of ca. 11% corresponding to the loss of the water of crystallization (11.3%, theoretical). This process is followed by a plateau of stability from 150−670 °C, followed by a rapid loss of coordinated water and ligands to provide an amorphous gray material.

The thermal diffraction profiles shows that a complete loss of water of crystallization results in decomposition of the material, which shows only broad, ill-resolved peaks above ca. 120 °C. It appears that the compounds of this study are unstable to the loss of solvent of crystallization, a process that results in framework collapse.

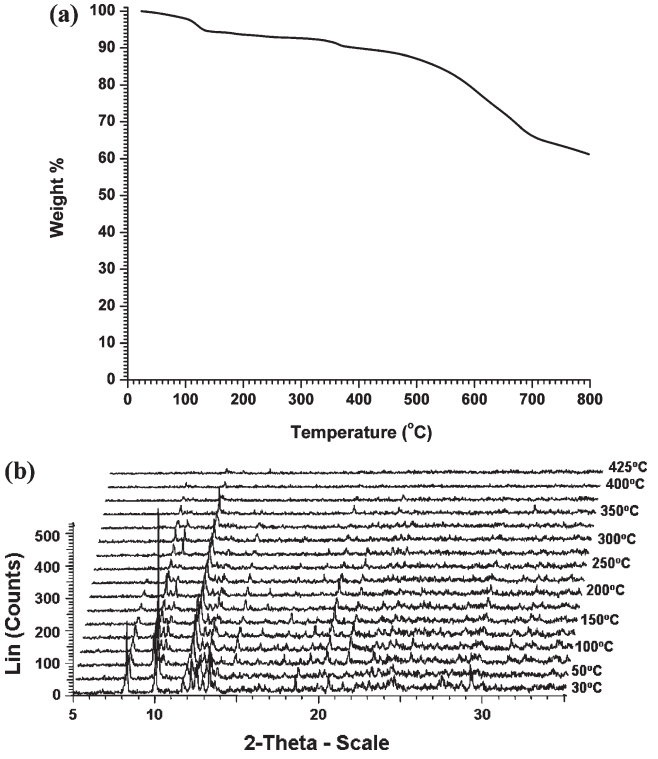


**Figure 10.** (a) Thermogravimetric analysis (TGA) curve for **4** in the 20−800 °C range. (b) Thermodiffraction pattern for **4** in the 30−425 °C temperature range.

**Magnetism.** The temperature-dependent magnetic susceptibilities of the majority of the compounds of this study were investigated. The data were analyzed using the isolated Heisenberg dimer model with the interaction Hamiltonian $H = -2JS_1 \cdot S_2$. For the copper(II) dimers, **2**, **3**, **5**, **7**−**9**, $S = 1/2$, while for the nickel(II) species, **6**, $S = 1$.[77,78] The presence of paramagnetic impurities in all samples of compound **1** precluded meaningful interpretation of its magnetic properties. The total contributions to the paramagnetism of the compounds **2**−**5** and **7**−**9** derive from the $\{Cu_2(bpyr)\}^{4+}$ units and that of **6** from the $\{Ni_2(bpyr)\}^{4+}$ group since the molybdenum sites of all compounds are exclusively Mo(VI) ($d^0$) and consequently diamagnetic.

The dependence of the magnetic susceptibility $\chi$ and effective magnetic moment $\mu_{eff}$ on the temperature for **3** is shown in Figure 11. The effective magnetic moment, $\mu_{eff} = \sqrt{(8\chi T)}$, increases with increasing temperature and reaches a value of $2.62\mu_B$ at 300 K, which corresponds to two $d^9$ $Cu^{2+}$ ions. The effective magnetic moment at 3 K is $0.31\mu_B$, indicating a singlet ground state ($S = 0$) arising from antiferromagnetic coupling. Taking into account the presence of monomeric impurities that obey the Curie−Weiss expression, the magnetic data were fit to eq 1 by a nonlinear least-square procedure that weights the data so that the percent difference deviation is minimized. $\rho$ and $\chi_{TI}$ represent the impurity fraction and the temperature-independent magnetic component, while $N$ = Avogadro's constant, $k_B$ is the Boltzmann constant,

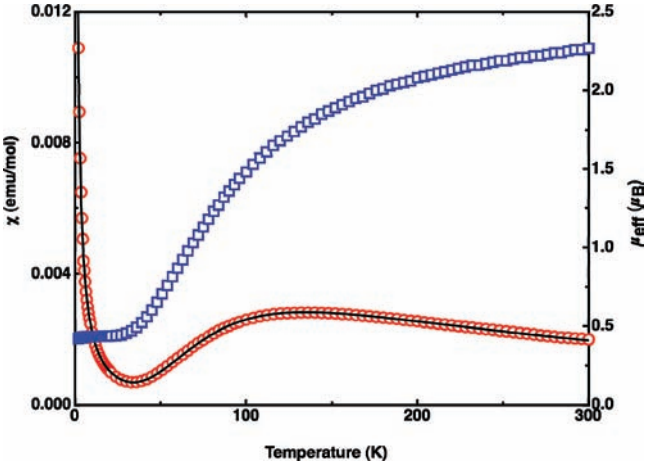


**Figure 11.** The temperature dependence of the magnetic susceptibility $\chi$ (red circles) and of the effective magnetic moment $\mu_{eff}$ (blue circles) of **3**.

and $\mu_B$ is the Bohr magneton.

$$\chi = \chi_0 + \chi_{TI} = (1-\rho)\frac{Ng^2\mu_B^2}{kT}\frac{2e^{2x}}{1+3e^{2x}} + \rho\frac{Ng^2\mu_B^2 S(S+1)}{3k(T-\theta)} + \chi_{TI} \quad (1)$$

The best fit was obtained for $g = 2.10$, $J/K = -122.2$ K, $\rho = 0.058$, $\Theta = -0.18$ K, and $\chi_{TI} = -1.000149$ emu/mol. The magnetic data for compounds **4**, **7**, and **8** were also fit to eq 1, and the best fit parameters are summarized in Table 3.

In the cases of compounds **2**, **5**, **6**, and **9**, the best fit was obtained by correcting the susceptibility from eq 1 for the exchange interaction $zJ'$ between spins, given in eq 2. In this case, the $\Theta$ term in eq 1 is taken to be 0.

$$\chi' = \frac{\chi_0}{1-(2zJ'/Ng^2\mu_B^2)\chi_0} \quad (2)$$

The thermal dependence of $\chi$ and of $\mu_{eff}$ for compound **2** are shown in Figure 12. The magnetic data for all compounds is summarized in Table 3.

For the copper-containing series of materials, the $J/K$ parameters clearly reveal strong antiferromagnetic coupling for compounds **3**, **4**, **5**, **7**, and **8** and much weaker coupling for compounds **2** and **9**. As shown in Figure 13, the magnitude of the antiferromagnetic coupling reflects the orientation of the copper basal or equatorial plane, for the "4 + 1" and "4 + 2" axially distorted geometries, relative to the bipyrimidine plane. Thus, when the equatorial planes of the two copper atoms of the $\{Cu_2(bpyr)\}^{4+}$ unit contain the *cis*-Cu−N bonds to the bipyrimidine ligand and are essentially coplanar with the bipyrimidine plane, the overlap between $d_{x^2-y^2}$ magnetic orbitals on each metal through the bridging bipyrimidine ligand results in strong antiferromagnetic coupling. This efficiency of the $\sigma$ in-plane exchange pathway through the ligand has been invoked to account for such strong coupling.[79,80] In contrast, for compounds **2**

(76) O'Connor, C. J. *Prog. Inorg. Chem.* **1979**, *29*, 203.
(77) Carlin, R.L. *Magnetochemistry*; Springer-Verlag: New York, 1986.
(78) Kahn, O. *Molecular Magnetism*; VCH Publishers: New York, 1993.
(79) Julve, M.; DeMunno, G.; Bruno, G.; Verdaguer, M. *Inorg. Chem.* **1988**, *27*, 3160.
(80) DeMunno, G.; Julve, M.; Lloret, F.; Cano, J.; Canesche, A. *Inorg. Chem.* **1995**, *34*, 2048.

**Table 3.** Summary of Magnetic Properties for Compounds **2**−**9**

| compound | **2** | **3** | **4** | **5** | **6** | **7** | **8** | **9** |
|---|---|---|---|---|---|---|---|---|
| $g$ | 2.12 | 2.10 | 2.28 | 2.28 | 2.29 | 2.16 | 2.13 | 2.28 |
| $J/K$ (K) | −3.4 | −112.2 | −112.0 | −124.3 | −11.6 | −123.2 | −121.0 | −7.1 |
| $J$ ($cm^{-1}$) | −2.4 | −77.9 | −83.3 | −86.4 | −8.1 | −85.5 | −84.0 | −4.9 |
| $\rho$ | 0.024 | 0.038 | 0.019 | 0.038 | 0.0022 | 0.018 | 0.025 | 0.065 |
| $\Theta$ (K) | | −0.18 | −2.71 | | | −1.59 | −2.60 | |
| $\chi_{TI}$ (emu/mol) | 0.000108 | −0.000149 | −.000186 | 0.000801 | 0.000094 | −0.000021 | −0.000179 | −0.000271 |
| $zJ'/k$ (K) | −0.5 | | | 11.1 | −0.5 | | | −6.6 |

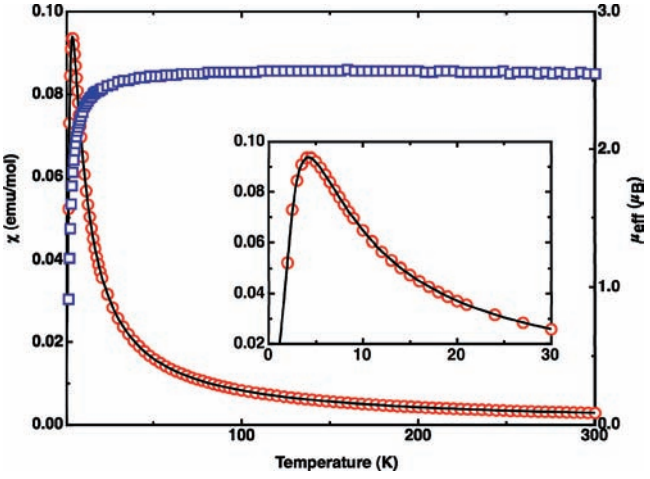


**Figure 12.** The temperature dependence of the magnetic susceptibility $\chi$ (red circles) and of the effective magnetic moment $\mu_{eff}$ (blue circles) of **2**.

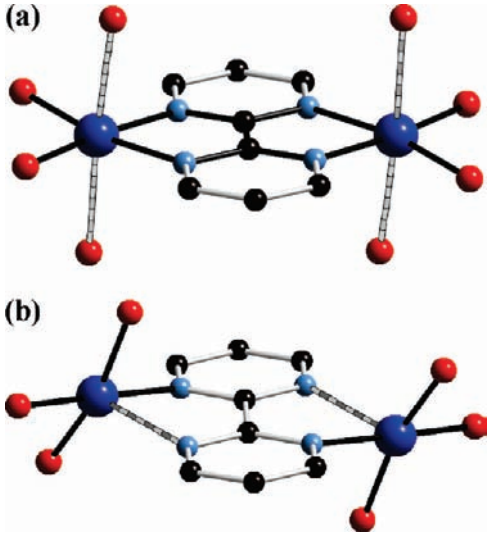


**Figure 13.** Schematic representations of the orientations of the copper coordination spheres relative to the ligand planes for (a) **3**, **4**, **5**, **7**, and **8** and (b) **2** and **9**. The striped Cu−N bonds define the long axial bonds or the $z$ axis of the copper polyhedra.

and **9**, the magnetic orbitals are canted at angles of 70.5° and 66.8° relative to the bipyrimidine, with the concomitantly significantly reduced antiferromagnetic coupling. In these instances, the equatorial planes of the Cu sites are defined by $\{CuNO_3\}$ coordination in contrast to the $\{CuN_2O_2\}$ equatorial planes of **3**, **4**, **5**, **7**, and **8**, as indicated by the differences in the Cu−N bond distances for **2** and **9** compared to those for **3**, **4**, **5**, **7**, and **8**. For compound **4**, the outer Cu pairs exhibit coplanarity of the bipyrimidine plane with the metal $d_{x^2-y^2}$ orbitals, while the magnetic orbitals for the central pair are canted. Consequently, the magnetism conformed to two separate Cu(II) dimers. Attempts to fit to a linear tetramer with the interaction Hamiltonian $H = 2J_1(S_1S_2 + S_3S_4) - 2J_2S_2S_3$ gives a $J_2$ that is essentially zero, confirming that there is no communication through the central pair of Cu sites of the tetramer.

It is noteworthy that, in the case of the Ni(II) material **6**, the magnetic orbitals are canted as for **2** and **9** and the value of $J/K$ is −11.6 K. However, as anticipated for a cation not influenced by a Jahn−Teller distortion, the range of Ni−ligand bond lengths is quite narrow in comparison to those observed for the Cu(II) compounds. In fact, previously reported examples of Ni(II) complexes of bipyrimidines[81−85] exhibit $J$ values in the range −6 to −16 $cm^{-1}$. This observation may simply reflect that the energies of the Cu(II) orbitals are lower than those of Ni(II), allowing greater spin density delocalization on the bridge and a larger $|J|$ value for the exchange pathway.[85] Compound **6** of this study exhibits a $J$ value at the lower end of the range for Ni(II)−bipyrimidines which may reflect the canting of the $d_{x^2-y^2}$ orbitals.

These results are similar to those reported for other examples of binuclear Cu(II)−bipyrimidine complexes. As shown in Table 4, $[Cu_2(bpyr)(C_4O_4)_2(H_2O)_6]$, $[Cu_2(bpyr)(C_5O_5)_2(H_2O)_2]\cdot 4H_2O$, $[Cu_2(bpyr)(H_2O)_4(SO_4)_2]\cdot 3H_2O$, $[Cu_2(bpyr)(NO_3)_4]$, $[Cu_2(bpyr)(malonate)_2(H_2O)\cdot 4H_2O$, and $[Cu(bpyr)(Cu_2O_7)]$ exhibit values of $J$ in the −147 to −191 $cm^{-1}$ range.[86−90] All possess small dihedral angles between the mean equatorial plane of the copper and the bipyrimidine plane. In contrast, $[Cu(bpyr)(SO_4)]\cdot H_2O$ is similar to **2** and **9** in that the plane of the magnetic orbital forms a large dihedral angle with respect to the bipyrimidine plane, to give a much reduced value for $J$ of −38 $cm^{-1}$.

(81) Brewer, G.; Sinn, E. *Inorg. Chem.* **1985**, *24*, 4580.
(82) DeMunno, G.; Julve, M.; Lloret, F.; Derory, A. *J. Chem. Soc.* **1993**, 1179.
(83) Colacio, E.; Lloret, F.; Navarrete, M.; Romerosa, A.; Stoeckli-Evans, H.; Suarez-Valera, J. *New J. Chem.* **2005**, *29*, 1189.
(84) Martin, S.; Barandika, M.; Cortes, R.; Ruiz de Larramendi, J. I.; Urtiaga, M.; Lezama, L.; Arriortua, M.; Rojo, T. *Eur. J. Inorg. Chem.* **2001**, 2107.
(85) Julve, M.; DeMunno, G.; Bruno, G.; Verdaguer, M. *Inorg. Chem.* **1988**, *27*, 3160.
(86) Castro, I.; Sletten, J.; Glaerum, L. K.; Cano, J.; Lloret, F.; Faus, J.; Julve, M. *J. Chem. Soc., Dalton Trans.* **1995**, 3207.
(87) Castro, I.; Sletten, J.; Glaerum, L. K.; Lloret, F; Faus, J.; Julve, M. *J. Chem. Soc., Dalton Trans.* **1994**, 2777.
(88) Spek, A. L. *Acta Crystallogr., Sect. A* **1995**, *28*, 659.
(89) DeMunno, G.; Bruno, G. *Acta Crystallogr., Sect. C* **1984**, *640*, 2030.
(90) Rodriguez-Martin, Y.; Sanchez, J.; Ruiz-Perez, C.; Lloret, F.; Julve, M. *Inorg. Chim. Acta* **2001**, *326*, 20.

**Table 4.** Selected Magnetostructural Data for Materials Containing Bipyrimidine-Bridged Cu(II) Sites

| compound | Cu···Cu (Å) | Cu−N (Å), eq. | Cu−N (Å), axial | Cu−O (Å), eq. | Cu−O (Å), axial | $\gamma$ (deg) | $J$ ($cm^{-1}$) |
|---|---|---|---|---|---|---|---|
| $\{Cu_2(bpyr)(malonate)_2(H_2O)_2]$ | 5.445(1) | 2.04 | | 1.90 | | 6.5 | −149 |
| $\{Cu_2(bpyr)(C_2O_4)_2(H_2O)_6]$ | 5.542(1) | 2.07 | | 1.96 | | 11.4 | −139 |
| $[Cu_2(bpyr)(C_5O_5)_2(H_2O)_2]$ | 5.384(1) | 2.02 | | 1.97 | | 14.4 | −160 |
| $[Cu_2(bpyr)(SO_4)_2(H_2O)_4]$ | 5.456(1) | 2.04 | | 1.97 | | 5.1 | −159 |
| $[Cu_2(bpyr)(NO_3)_4]$ | 5.371(1) | 2.01 | | 1.96 | | 3.5 | −191 |
| $[Cu(bpyr)(Cu_2O_7)]$ | 5.486(2) | 2.04 | | 1.93 | | | −147 |
| $[Cu(bpyr)(SO_4)]$ | 5.648(1) | 2.05 | | 1.95 | | | −38 |
| **2** | 5.699(1) | 2.005 | 2.321 | 1.947 | | | −2.4 |
| **3** | 5.435(1) | 2.032 | | 1.893 | 2.369 | | −77.9 |
| **4** | 5.496(1) | 2.046 | | 1.944 | 2.393 | | −83.3 |
| | 5.663(1) | 1.990 | 2.208 | 2.040 | 2.243 | | |
| **5** | 5.458(1) | 2.039 | | 1.964 | 2.374 | | −86.4 |
| **7** | 5.475(1) | 2.042 | | 1.945 | 2.244 | | −85.5 |
| **8** | 5.474(1) | 2.036 | | 1.956 | 2.325 | | −84.0 |
| **9** | 5.763(1) | 2.009 | 2.336 | 1.956 | | | −4.9 |

## Conclusions

Hydrothermal synthesis has been exploited to prepare a series of compounds of the copper(II)−bipyrimidine/$Mo_xO_y$−organophosphonate family and one example of a nickel(II)-containing material. In common with previously described materials of the M(II)-binucleating ligand/$Mo_xO_y$−organophosphonate class, the structures of the materials are characterized by the presence of oxomolybdate−phosphonate clusters acting as nodes, with $\{Cu_2(bpyr\}^{4+}$ rods serving to link the nodes to provide spatial expansion of the structures.

The structural chemistry of the Cu(II)−bipyrimidine/$Mo_xO_y$−organophosphonate compounds of this study reveals the persistence of the $\{Mo_5O_{15}(O_3PR)_2\}^{4-}$ cluster, which is observed in all cases save for $[\{Cu_2(bpyr)\}MoO_2(O_3PCH_2PO_3)_2]\cdot 2H_2O$ (**3**·$2H_2O$). In the case of **3**, it is the coordination requirements of the methylenediphosphonate ligand, which chelates to a single molybdenum site rather than providing spatial extension between nodes, that provide the structural determinism, as noted previously.

While the Cu(II)−bipyrimidine subunit was generally present in these structures as the anticipated $\{Cu_2(bpyr)\}^{4+}$ rod and functioning as a tether between molybdate nodes, the tendency of M(II)−bipyrimidine units to catenate was revealed in the $\{Cu(bpyr)\}_n^{2n+}$ chain of $[\{Cu(bpyr)\}_2Mo_5O_{15}(O_3PCH_3)_2]\cdot 2.5H_2O$ (**1**·$2.5H_2O$) and in the $\{Cu_4(bpyr)_3(H_2O)_6\}^{8+}$ clusters of **4**·$4H_2O$. Observations such as these highlight the problematic nature of structural predictions for these multicomponent systems. While it is predictable that, when exploiting diphosphonates $\{O_3P(CH_2)_nPO_3\}^{4-}$ with $n \geq 2$, the characteristic $[Mo_5O_{15}\{O_3P(CH_2)_nPO_3\}]_n^{4n-}$ chains will form; the numbers and locations of M(II)-binucleating ligand linkers associated with a given phosphomolybdate cluster are variable, reflecting influences such as charge density matching,[91] steric, and packing considerations. To these variables can be added the possibility of catenation of the M(II)-binucleating ligand subunits, as observed for $\{Cu(bpyr)\}_n^{2n+}$ and $\{Cu_4(bpyr)_3(H_2O)_4\}^{8+}$ for **1** and **4** of this study and of $\{Ni_4(tpyprz)_3\}^{8+}$ (tpyprz = tetrapyridylpyrazine) of the previously reported $[\{Ni_4(tpyprz)_3\}Mo_5O_{15}\{O_3PCH_2CH_2PO_3\}_2]\cdot 23H_2O$. While some structural systematics continue to emerge for these complex materials, the inherent structural variability of the component nodes and tethers continues to render total predictability of structure rather problematic.

**Acknowledgment.** This work was supported by a grant from the National Science Foundation (CHE-0604527). The magnetic studies were made possible by a grant from the Defense Advanced Research Projects Agency (Grant MDA972-04-1-0029). E.R. acknowledges support from the Louisiana Board of regents through contract number LEQSF(2007-12)-ENH-RKSFI-PRS-04.

**Supporting Information Available:** Tables of atomic positional parameters, bond lengths, bond angles, anisotropic temperature factors, and calculated hydrogen atom positions for **1**−**9** in CIF format. ORTEP diagrams for **1**−**9** and views of the cavities occupied by water of crystallization for **3**, **5**, and **8** (Supplementary Figures S1−S12). TGA profiles, thermal diffraction plots, and magnetic susceptibility plots for **1**−**9** (Supplementary Figures S13−S33). This material is available free of charge via the Internet at http://pubs.acs.org.

(91) Maggard, P. A.; Bodyle, P. D. *Inorg. Chem.* **2003**, *42*, 4200.